Utrecht University

Faculty of Science

Pattern Formation on Progressively less Regular Networks

Master Thesis

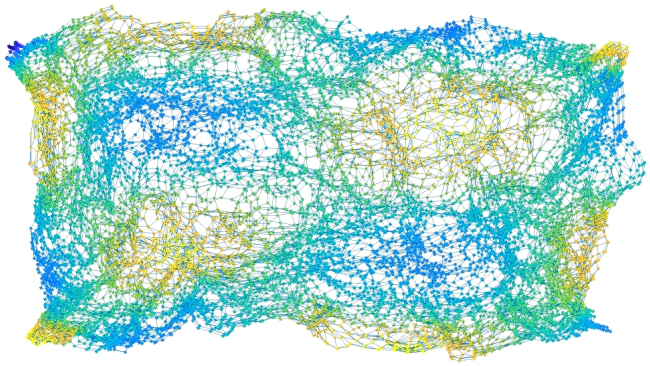

Supervisors
Dr. R. Bastiaansen
Mathematical Institute, UU
Dr. I.V. Kryven
Mathematical Institute, UU

Author
M. Spoorenberg
5730988

Friday 17th May, 2024

Abstract

The world is getting smaller. Globalization and climate change have a great impact on the spreading of species and their resources. Shifting climate zones affect habitats and ecosystems, which in turn changes the effective distances within these systems. Interactions between different species and their resources that were previously local can now take place over greater distances. Reaction diffusion equations are used to model spatial systems that involve interactions like ecosystems. The equations are usually posed on a two-dimensional plane, discretised into a regular lattice, but in real life, the interactions are not necessarily local. Also domains can be more complicated than a plane, like a network for instance. On the lattice, as well as on the network, Turing instabilities can cause pattern formation. In this thesis we bridge part of the gap between a two-dimensional spatial domain and a three-dimensional network by studying Turing instabilities from Gray-Scott/Klausmeier type reaction diffusion equations posed on progressively less regular networks. We combine analytic and numerical methods make the transition from a continuous model to discretised equations. A linear stability analysis of the discretised reaction diffusion system near the Turing bifurcation leads to the derivation of a discrete dispersion relation that links the unstable eigenfunctions of the full system to the eigenvalues of the discrete Laplacian.

Findings show that unstable, increasingly coarse patterns are emerging on the increasingly less regular networks. Like in the continuous case, the unstable patterns can be predicted by the dispersion relation. The results demonstrate that the unstable eigenvectors for the less regular three-dimensional networks often correspond to analytically derived eigenfunctions for smaller continuous two-dimensional domains. In the ecological setting this would imply that more connected ecosystems behave similar to smaller scaled ecosystems, and might be less resilient due to restricted patterning options.

Keywords: *Reaction-diffusion system - Networks - Turing bifurcation - Pattern formation*

Contents

1 Introduction

We are surrounded by patterns. Some are very small, like the facet eyes of a fly (Kim et al. 2016) or shape of ice-crystals (Libbrecht 2003), some are very large like dunes in the desert (Herzog et al. 2022), (Herrmann 2006) or the shape of a spiral galaxy (Carlberg and Freedman 1985). People have a tendency to look for patterns, trying to find explanations for the world that surrounds them.
Since patterns can occur for very different reasons, there is not a single mechanism that can describe all off them. Some are caused by external forces, and others arise from internal processes. There may also be several explanations for a single pattern formation. In biology, for example, where stripes on animal coats can have an evolutionary origin, but the actual creation of the pattern on each individual is determined chemically.

With the publishing of 'The chemical basis of morphogenesis' in 1952 (Turing 1952), Alan Turing proposed a way to model these and other patterns by describing how they could arise from instabilities in the uniform state of a system. In his model, Turing combined diffusion with reactions between different chemicals.
Diffusion itself is the spreading out of chemicals that eventually makes the system homogeneous. Reactions can lead to a stable equilibrium where the system is also homogeneous. But introducing diffusion into a reaction model can destabilise the system. A small perturbation of the homogeneous system will start to grow instead of damping out. This causes local increase or decrease of the density of one or more chemicals, and a heterogeneous state of the system arises. Today, these patterns are called *Turing patterns*.

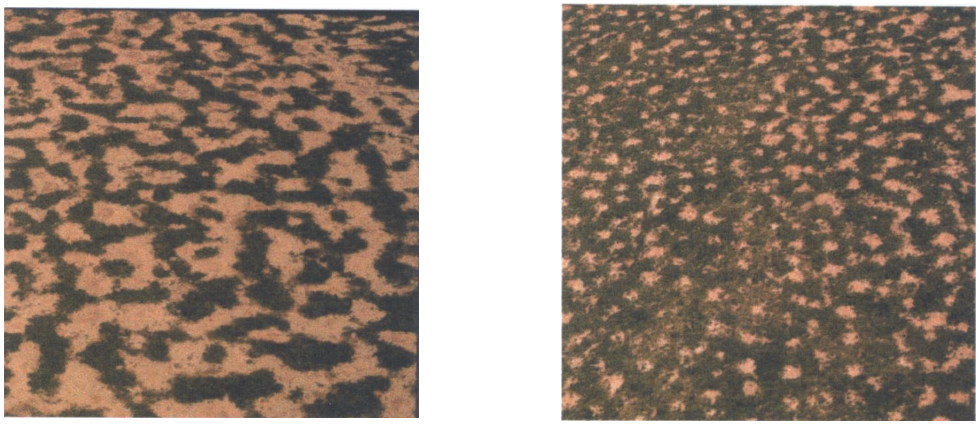

(a) (b)

Figure 1: Labyrinth (a) and gap pattern (b) in patterned vegetation in arid areas (Rietkerk et al. 2002)
.

One of the most striking examples of Turing patterns is the phenomenon of pattern formation in arid areas (Max Rietkerk, Dekker, et al. 2004), (Sherratt and Lord 2007). The patterns are clearly visible, even from space, and are formed by alternating patches of plants and bare soil resulting in spotted vegetation, labyrinths (Figure 1a), gap patterns (Figure 1b), and regular bands (Rietkerk et al. 2002). The patterns are the result of spatial self-organization, resulting from the feedback mechanisms between biomass and water. Unlike bare soil, vegetated patches facilitate water infiltration, leading to higher water concentrations in vegetated patches and lower ones in bare soil. As the climate changes, the patterned ecosystems respond to changes in the precipitation by making a transition to another patterned state or to the bare state (Siteur et al. 2014), (Bastiaansen, Doelman, et al. 2020).
One of the models used to study the vegetation patterns is the Klausmeier model (Klausmeier 1999). In this model, the species represent water and vegetation density. This model is a reaction-advection-diffusion model. It was originally developed by Christopher A. Klausmeier. He modeled vegetation patterns as a result of the plants competition for water in semiarid regions. The model was later

adapted by van der Stelt et al. (Stelt et al. 2013). We will be using a simplified version of this model throughout this thesis, the model description of which will be given in Section 2.2.
Turing patterns have been considered an early warning signal that predicts catastrophic shifts in ecological systems but that assumption has been questioned recently. Instead there are indications that the formation of Turing patterns is a manifestation of resilience against tipping (Max Rietkerk, Bastiaansen, et al. 2021). Instead of reaching the tipping point, the system follows a pathway in which patterned states with different wavenumbers can coexist. These pathways lie in a parameter space defined by the Busse balloon (see Figure 2). Its starting point is the Turing point T.

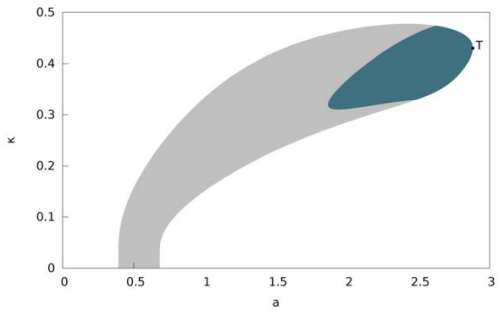

Figure 2: Busse balloon for the extended Klausmeier model. From (Siero et al. 2015).

In Turing's model, reactions are local and depend on the network of cells in which the reactions take place. These cells lie in a circle, which is basically a one-dimensional domain, with periodic boundary conditions. Patterns on such a domain can easily be visualised. Also on a two-dimensional domain, the visualisation of patterns does not pose serious problems. These kinds of domains, in their simplest form a line or a rectangle, are the most obvious forms to study. They are especially easy to discretise into a line of equally distant points, or a rectangular lattice, where species only interact with their closest neighbours. But in real life, interactions are not necessarily local, and boundary conditions may vary at different edges of the domain. Strange domain shapes and non-local interactions are quite common in the natural world, and regularity is not self-evident. The visualisation of the patterns would be more challenging and finding an analytical solution might no longer be possible. Human activities in particular can make reactions between species that were previously non-local now suddenly local, for example through the spread of plant seeds, exotic or native, via man-made infrastructures (Hodkinson and Thompson 1997). The domain might even be quite complicated, like a complex network (McCullen and Wagenknecht 2016).
In this thesis we bridge the difference between a reaction diffusion equation posed on a simple two-dimensional domain and on a more complicated network. By making a regular discretised lattice progressively less regular, we study the effect that the randomisation has on a reaction diffusion system. We also investigate a way to compare the numerically obtained results with analytical unstable eigenfunctions of the system.

The structure of the rest of the thesis is as follows.
In Section 2 the theory for the general reaction diffusion equations for a two component model posed on a two-dimensional bounded domain is introduced. Parallel to the general model we give a detailed stability analysis of the Klausmeier model, followed by the conditions for pattern formation and the derivation of the dispersion relation. We end this section with some examples of patterns generated with the Klausmeier model, and a warning that numerical computations of the unstable eigenfunctions do not always yield the same results.
Section 3 is divided into two parts. In the first part we will discretise the reaction diffusion system on the rectangular domain into a reaction diffusion system on a regular lattice. We analyse the stability of the discretised model against homogeneous and spatially heterogeneous perturbations.
In the second part of this section we will stepwise change the regular lattice into a less regular network.

We will establish the procedure and the rules that this process must comply with in Section 3.2.1. The changes to the domain will be implemented into the equations in such a way that we will be able to perform the same stability analysis for each subsequent network as we did in the case of the system on the regular lattice. We will find a sequence of destabilising eigenvalues for the sequence of networks. The corresponding eigenfunctions of the eigenvalues can be plotted onto the three-dimensional network, or projected onto the initial two-dimensional regular lattice. The latter will enable us to compare the eigenfunctions of the discretised network model with the continuous reaction diffusion model on a sequence of domains of different sizes. We will find that the discretised reaction diffusion equations posed on the network with ordered randomisation of edges yields analogous results as the analytic results for smaller continuous domains. We will use the diameter of the network as a metric to compare the size of the changing network to the size of the shrinking continuous domain.

2 Theory

In this section we will give a set-up for a general two-component set of reaction diffusion equations, posed on a continuous two-dimensional rectangular domain. We will analyse the stability of the homogeneous solutions to homogeneous and non-homogeneous perturbations. Once we have derived the eigenfunction-eigenvalue solutions of the system we will formulate the conditions for which pattern formation can occur and find the Turing point. We will simultaneously derive the results of the analysis for the Klausmeier model that is used throughout this thesis. In the main text body we treat the general model. In the boxes, the procedures from the main text are applied to the specific case of the Klausmeier model.

2.1 General reaction-diffusion system

Reaction diffusion equations are used to model the dynamics of systems with multiple components, sometimes called species. As can be deduced from the name, the changes in the system are caused by two different mechanisms. The change in species density is caused by their diffusion in space but also by the local interactions with each other. Due to the infinitesimal time intervals, modeling them into a differential equation makes their contributions to the rate of change become independent. This means that the contributions can easily be added and that the solution of the differential equation takes all mechanisms into account.
The basic reaction diffusion system in n dimensions consists of a set of m equations of the form;

$$\frac{\partial u}{\partial t} = d\triangle u + f(u) \tag{1}$$

with

$$u = \begin{pmatrix} u_1 \\ u_2 \\ . \\ . \\ u_m \end{pmatrix}, \quad d\triangle u = \begin{pmatrix} d_1\triangle u_1 \\ d_2\triangle u_2 \\ . \\ . \\ d_m\triangle u_m \end{pmatrix} \text{ and } \quad x = \begin{pmatrix} x_1 \\ x_2 \\ . \\ . \\ . \\ . \\ x_n \end{pmatrix}, \tag{2}$$

where u is the concentration of substances or species. The function $f : \mathbb{R}^m \to \mathbb{R}^m$ are the reaction kinetics that describe the local interactions between the species. The diagonal matrix d contains the diffusivity coefficients of the species $d_1, d_2, ..., d_m$, and $\triangle$ denotes the Laplace operator such that

$$\triangle = \frac{\partial^2}{\partial x_1^2} + \frac{\partial^2}{\partial x_2^2} + ... + \frac{\partial^2}{\partial x_n^2}. \tag{3}$$

A mathematical formulation of the problem requires boundary and initial conditions. Neumann boundary conditions allow the system to self-organise patterns whereas Dirichlet boundary conditions could force a pattern upon the domain. Therefore the domain Ω will in our case be bounded with no-flux boundary conditions at boundary $\partial\Omega$;

$$\left.\frac{\partial u}{\partial n}\right|_{\partial\Omega} = 0, \tag{4}$$

where n is the outward normal perpendicular to the boundary $\partial\Omega$ of the domain Ω.
The initial condition is

$$u(x, 0) = u_0. \tag{5}$$

2.2 Analysis of the two-component model in two spatial dimensions

The model that is used in this thesis is based on the two component Klausmeier model. The domain is restricted to two spatial dimensions where $\mathbf{x}$ is a two dimensional vector $(x, y) \in \Omega$ such that we

can define the bounded domain $\Omega = [0, p] \times [0, q]$ with $0 \leq x \leq p$, and $0 \leq y \leq q$. The general two-component reaction diffusion model on a two dimensional domain is defined as

$$\begin{cases} \dfrac{\partial u}{\partial t} = & \triangle u + f(u, v) \ , \quad \text{in } \Omega \times (0, T) \\ \dfrac{\partial v}{\partial t} = & \varepsilon^2 \triangle v + g(u, v) \ , \quad \text{in } \Omega \times (0, T). \end{cases} \tag{6}$$

In (6), Δ denotes the Laplace operator such that $\Delta = \dfrac{\partial^2}{\partial x^2} + \dfrac{\partial^2}{\partial y^2}$. Diffusivity coefficient ε^2 is the scaled diffusion applied to species v. The functions $f : \mathbb{R}^2 \to \mathbb{R}^2$ and $g : \mathbb{R}^2 \to \mathbb{R}^2$ are the nonlinear reaction kinetics of the model that describe the local interactions between u and v.
The initial conditions are

$$\begin{aligned} u(x, y, 0) &= u_0(x, y) \text{ in } \Omega \\ v(x, y, 0) &= v_0(x, y) \text{ in } \Omega, \end{aligned} \tag{7}$$

and the zero flux boundary conditions on domain Ω are

$$\left. \frac{\partial \phi(x, y)}{\partial n} \right|_{\partial \Omega} = 0, \tag{8}$$

where n is the outward normal perpendicular to the boundary $\partial\Omega$ of the domain Ω.

The Klausmeier model, model description

The model that is used throughout this thesis is the extended Klausmeier model. This model describes patterns in semi-arid ecosystems. It consists of two components that represent water u and vegetation v. The non-dimensionalised system of partial differential equations of the model is defined as

$$\begin{aligned} \frac{\partial u}{\partial t} &= \frac{d^2 u}{d\boldsymbol{x}^2} + c\frac{du}{d\boldsymbol{x}} + a - u - uv^2 \\ \frac{\partial d}{\partial t} &= \varepsilon^2 \frac{d^2 v}{d\boldsymbol{x}^2} - mv + uv^2, \end{aligned} \tag{9}$$

where $\boldsymbol{x}$ is the two-dimensional spatial variable (x, y).
Parameter ε^2 is the diffusivity of the vegetation variable v such that the diffusivity of variable u is scaled to 1. One can also think of $0 < \varepsilon < 1$ as a measure for the ratio of diffusion constants (Bastiaansen, Chirilus-Bruckner, and Doelman 2020). Parameter $a \geq 0$ represents the precipitation.
The infiltration of surface water into the soil is improved on patches where vegetation is growing. This is called infiltration feedback (Gilad et al. 2007). Together with the water uptake by the roots, the total water uptake $\pm uv^2$ is quadratic. Finally, $-u$ is the evaporation of water, and $m > 0$ is the mortality of the vegetation (Siero et al. 2015). The term $c\frac{du}{dx}$ models the advection which is used to model the flow of water on sloped terrain. It will not be used in this thesis so c is set to zero.
The initial conditions are

$$\begin{aligned} u(\boldsymbol{x}, 0) &= u_0(\boldsymbol{x}) \text{ in } \Omega \\ v(\boldsymbol{x}, 0) &= v_0(\boldsymbol{x}) \text{ in } \Omega \end{aligned}$$

and the zero flux boundary conditions are

$$\left. \frac{\partial \phi(x, y)}{\partial n} \right|_{\partial \Omega} = 0, \tag{10}$$

where n is the outward normal, perpendicular to the boundary $\partial\Omega$ of the domain Ω, like in the general case.

2.2.1 The homogeneous solution

In order to exhibit Turing instability, or more generally, *diffusion driven* instability, the homogeneous steady state of the system must be unstable to spatial perturbations only. The homogeneous solution is the time and space independent solution of the system. When u and v are spatially homogeneous, the diffusion is absent. That means that only the time-derivative remains and the system of partial differential equations now has become an ordinary differential equation. For time independence, we set

$$\begin{aligned} f(u,v) &= 0 \\ g(u,v) &= 0, \end{aligned}$$

which when solved yields the steady state solutions (u_*, v_*).

The Klausmeier model, the homogeneous solution

The homogeneous solutions of the Klausmeier model are found by solving

$$\begin{aligned} f(u,v) &= a - u - uv^2 = 0 \\ g(u,v) &= -mv + uv^2 = 0. \end{aligned}$$

The model has three stationary solutions (u_*, v_*)

$$\begin{aligned} A &= (a, 0), \\ B &= \left(\frac{a + \sqrt{a^2 - 4m^2}}{2}, \frac{2m}{a + \sqrt{a^2 - 4m^2}} \right), \\ C &= \left(\frac{a - \sqrt{a^2 - 4m^2}}{2}, \frac{2m}{a - \sqrt{a^2 - 4m^2}} \right). \end{aligned} \tag{11}$$

From a physical point of view, not all solutions are allowed. Both u and v must be real and positive to be biologically relevant. Therefore the following inequalities must be true

$$\begin{aligned} a &\geq 0 \\ m &\geq 0 \\ \sqrt{a^2 - 4m^2} &\geq 0 \Rightarrow a \geq 2m. \end{aligned} \tag{12}$$

In the case of the stationary solutions of the Klausmeier model there are three possibilities; (1) for $a < 2m$, only solution A will exist, (2) for $a = 2m$, there will be two solutions, A and B and (3) for $a > 2m$, all three solutions are possible. The phase diagrams in Figure 3 show how the nullclines change with different values of parameter a. The grey arrows indicate the vector field of the functions $f(u,v)$ and $g(u,v)$.

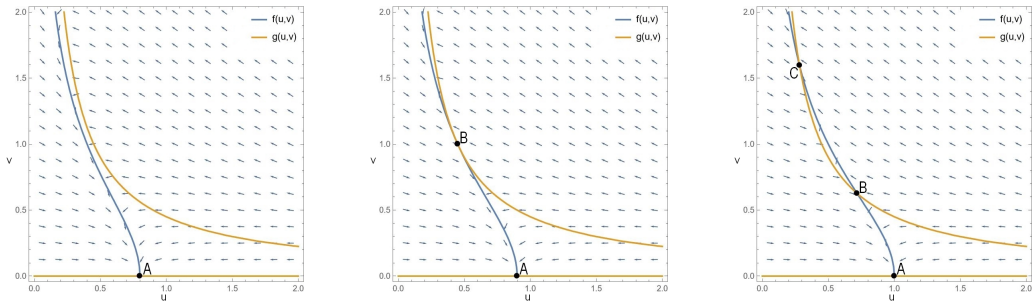

(a) (b) (c)

Figure 3: The kinetics nullclines $f = 0$ and $g = 0$ that show the existence of equilibrium points for $a < 2m$ in (a), $2m = a$ in (b) and $a > 2m$ in (c) *Mathematica*.

2.2.2 Linear stability to homogeneous perturbations

In the absence of diffusion, the homogeneous steady state must be linearly stable. In order to determine the stability of the steady states we define a perturbation

$$\mathbf{w} = \begin{pmatrix} \bar{u} \\ \bar{v} \end{pmatrix} = \begin{pmatrix} u - u_* \\ v - v_* \end{pmatrix}, \tag{13}$$

with $|\mathbf{w}|$ small. Then we linearise the equations around the equilibrium state (u_*, v_*) such that the first order Taylor polynomial of the uniform model is

$$\begin{aligned} \frac{\partial \bar{u}}{\partial t} &\approx f_u(u_*, v_*)\bar{u} + f_v(u_*, v_*)\bar{v} \\ \frac{\partial \bar{v}}{\partial t} &\approx g_u(u_*, v_*)\bar{u} + g_v(u_*, v_*)\bar{v}. \end{aligned} \tag{14}$$

In matrix form this can be written as;

$$\begin{pmatrix} \frac{\partial \bar{u}}{\partial t} \\ \frac{\partial \bar{v}}{\partial t} \end{pmatrix} = J \begin{pmatrix} \bar{u} \\ \bar{v} \end{pmatrix}, \text{ with } J = \begin{pmatrix} f_u & f_v \\ g_u & g_v \end{pmatrix}_{(u_*, v_*)}. \tag{15}$$

or more compactly

$$\bar{\mathbf{w}}_t = J\bar{\mathbf{w}}. \tag{16}$$

Vector $\bar{\mathbf{w}}_t$ is the time derivative of $\bar{\mathbf{w}}$, and matrix J is the Jacobian or stability matrix at the equilibrium point (u_*, v_*).

The Klausmeier model

If we apply the Taylor approximations to the Klausmeier model, the specific equations become

$$\begin{aligned} \frac{\partial \bar{u}}{\partial t} &\approx (-1 - v^2)\bar{u} - 2uv\bar{v} \\ \frac{\partial \bar{v}}{\partial t} &\approx v^2\bar{u} + (2uv - m)\bar{v}. \end{aligned} \tag{17}$$

The Jacobian matrix of the compact form $\bar{\mathbf{w}}_t = J\bar{\mathbf{w}}$ can now be specified as

$$J = \begin{pmatrix} f_u & f_v \\ g_u & g_v \end{pmatrix} = \begin{pmatrix} -(1 + v^2) & -2uv \\ v^2 & -m + 2uv \end{pmatrix}_{(u_*, v_*)}. \tag{18}$$

To solve equation (16) we perform a separation of variables.

$$\mathbf{w}(t) = \psi(t)\mathbf{w} \tag{19}$$

Substituting (19) into (16) and dividing both sides by $\psi(t)$ yields

$$\frac{\psi'(t)}{\psi(t)}\mathbf{w} = J\mathbf{w}. \tag{20}$$

Because the right hand side of (20) is time independent, the equation only holds if the term $\frac{\psi'(t)}{\psi(t)}$ is constant. Substituting the *Ansatz*

$$\psi(t) = \psi(0)e^{\lambda t}, \tag{21}$$

into (20) results in the eigenvalue problem

$$\lambda\mathbf{w} = J\mathbf{w}, \tag{22}$$

with eigenvalues λ_i and their corresponding eigenvector $\mathbf{w_i}$, $i = 1, 2$.
If the real part of λ_i is smaller than zero, then the value of the time dependent part of the perturbation (21) will go to zero as t goes to infinity and the solution is linearly stable.
The characteristic equation $\det(J - \lambda I) = 0$ leads to the derivation of both eigenvalues;

$$\begin{aligned}\lambda_1, \lambda_2 &= \frac{1}{2}\left[(f_u + g_v) \pm \sqrt{(f_u + g_v)^2 - 4(f_u g_v - f_v g_u)}\right] \\ &= \frac{1}{2}\left[\mathrm{tr}(J) \pm \sqrt{(\mathrm{tr}(J))^2 - 4\det(J)}\right]. \end{aligned} \tag{23}$$

As mentioned before, in order for the steady states to be stable, the real part of the eigenvalues λ_1 and λ_2 of matrix J at steady state (u_*, v_*) must be smaller than zero. This is the case if the determinant of the Jacobian is positive and the trace is negative. All four possible combinations for the sign of the trace and the determinant and the signs of the real parts of both eigenvalues can be found in Table 1.

Table 1: Combinations of the signs of the trace and determinant J and the absolute values of the real part of the eigenvalues of the Jacobian matrix J.

	$\mathrm{trace}(J) < 0$	$\mathrm{trace}(J) > 0$
$\det(J) > 0$	$\mathrm{Re}(\lambda_+) < 0$ $\mathrm{Re}(\lambda_-) < 0$	$\mathrm{Re}(\lambda_+) > 0$ $\mathrm{Re}(\lambda_-) > 0$
$\det(J) < 0$	$\mathrm{Re}(\lambda_+) > 0$ $\mathrm{Re}(\lambda_-) < 0$	$\mathrm{Re}(\lambda_+) > 0$ $\mathrm{Re}(\lambda_-) < 0$

Following from Table 1, the conditions for linear stability of the uniform steady states in terms of f_u, g_v,f_v and g_u are;

$$1. \qquad f_u g_v - f_v g_u > 0 \tag{24}$$

$$2. \qquad f_u + g_v < 0 \tag{25}$$

The Klausmeier model

The stability of the three steady states A, B and C against homogeneous perturbations can be investigated by applying the previous theory to the Klausmeier model. At steady state A, the Jacobian matrix reads

$$J_A = \begin{pmatrix} -1 & 0 \\ 0 & -m \end{pmatrix}. \tag{26}$$

The real part of both eigenvalues of this matrix is always negative, therefore state A is always stable. From an ecological point of view, this is a bare landscape without any vegetation.

The Jacobian matrix for steady states B and C is identical;

$$J_{B,C} = \begin{pmatrix} -1 - v_*^2 & -2m \\ v_*^2 & m \end{pmatrix}_{(u_*, v_*)} \tag{27}$$

First we consider the linear stability of state B,

$$B = \left(\frac{a + \sqrt{a^2 - 4m^2}}{2}, \frac{2m}{a + \sqrt{a^2 - 4m^2}} \right).$$

The sign of the determinant of the Jacobian at B only depends on the values of v_B^2.

$$\begin{aligned} \det(J_B) &= (-1 - v_B^2)m - v_B^2(-2m) \\ &= m(v_B^2 - 1) \end{aligned} \tag{28}$$

The inequality $v_B > 1$ forms the lower bound if we want that $\det(J_B) > 0$.
We can also derive the upper bound of v_B by first looking at the value of u_B. From (12) we know that $a \geq 2m$ and therefore that $u_B \geq m$. If we multiply u_B with v_B we can derive the expression $v_B = \frac{m}{u_B}$. But since $u_B \geq m$ we find that $v_B \leq 1$ and therefore that the determinant of the Jacobian $\det(J_B) = m(v_B^2 - 1) \leq 0$ and the system is not stable. For the case where $a < 2m$, we find that $\det J_B = 0$ and therefore B is a saddle point and will always be unstable.
Lastly we determine the stability of state C

$$C = \left(\frac{a - \sqrt{a^2 - 4m^2}}{2}, \frac{2m}{a - \sqrt{a^2 - 4m^2}} \right). \tag{29}$$

The stability of C will depend on the value of v_C for which we can derive an upper bound. By rewriting v_C as

$$v_C = \frac{a}{2m} + \frac{1}{2m}\sqrt{a^2 - 4m^2}) \tag{30}$$

and using $a \geq 2m$ (12) it becomes clear that $\frac{a}{2m} \geq 1$ and therefore $v_C \geq 1$. The determinant of the Jacobian at steady state C is now

$$\det(J_C) = m(v_0^2 - 1) \geq 0 \tag{31}$$

which satisfies (24). But the real part of the eigenvalues can still be positive or negative. To resolve this we look at the trace of Jacobian at C. We have that $\text{trace}(J_C) = -1 - v_C^2 + m$ and this must be smaller than zero. Because of the constraint that $v \geq 0$ to be physically relevant, the trace is indeed smaller than zero if $m < 1$. Up to when $m \leq 2$, the trace will be negative automatically. But when m is larger then 2, there is another constraint to the parameters. We know that for linear stability for stable state C we must have that

$$\begin{aligned} \text{trace} J_C &= -1 - v_C^2 + m = -1 - \left(\frac{a + \sqrt{a^2 - 4m^2}}{2m} \right)^2 + m \leq 0 \\ \Rightarrow m - 1 &\leq \left(\frac{a + \sqrt{a^2 - 4m^2}}{2m} \right)^2 = \frac{2a\sqrt{a^2 - 4m^2} + 2a^2}{4m^2} - 1 \\ \Rightarrow 2m^3 &\leq a\sqrt{a^2 - 4m^2} + a^2 \\ \Rightarrow a &\geq \frac{m^2}{\sqrt{m-1}}. \end{aligned} \tag{32}$$

So when $m \geq 2$, condition $a \geq 2m$ is not strong enough anymore for the steady state to be stable. Instead the constraint is not $a \geq 2m$ but $a \geq \frac{m^2}{\sqrt{m-1}}$. The parameter space for these stronger bonds is displayed in Figure 4.

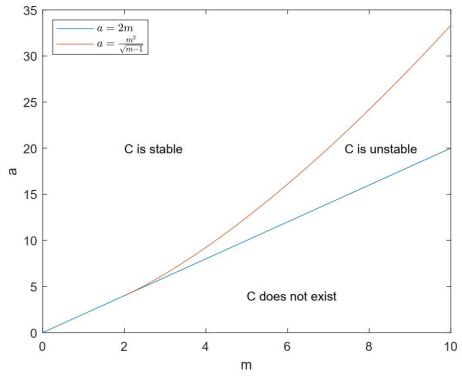

Figure 4: Parameter space of a and m for which state C is stable and unstable.

Changes in stability, or bifurcations, can be made visible with a bifurcation diagram. The bifurcation diagram of the Klausmeier model with parameter value $m = 0.45$ is given in Figure 5. The change of a parameter of the model causes the passing of the real part of an eigenvalue through zero. In that case, the stability of an equilibrium, or fixed point, changes. In the case of the Klausmeier model, when parameter a is reduced to the critical point $a = 0.9$, a catastrophic transition causes the vegetation v to disappear entirely. Only bare state A remains and the transition can not be reversed by increasing parameter a.

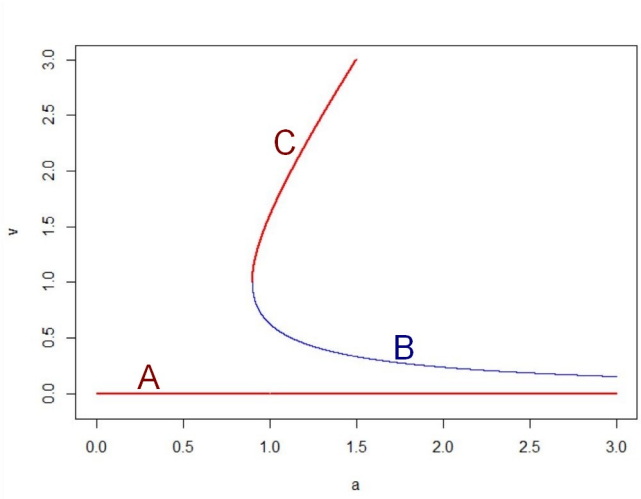

Figure 5: The bifurcation diagram of the Extended Klausmeier model for $m = 0.45$ with curves for stable state without vegetation A, unstable saddle node B and stable state C. When the decreasing parameter a reaches the tipping point at $a = 0.9$, a catastrophic transition occurs. States C and B disappear and only stable state A remains in which case there is no species v. Increasing a will not reverse the transition.

2.2.3 Linear stability to spatially heterogeneous perturbations

Returning to the full reaction diffusion model, the spatial component makes the system also subject to heterogeneous perturbations. In the case of the Klausmeier model state C, that was stable against homogeneous perturbation may be unstable against spatial perturbations. If diffusion causes a spatial instability of the uniform system, pattern formation can occur.

The full system can be linearised about the steady state (u_*, v_*) with $\mathbf{w} = \begin{pmatrix} \bar{u} \\ \bar{v} \end{pmatrix} = \begin{pmatrix} u - u_* \\ v - v_* \end{pmatrix}$, for a small perturbation $|\mathbf{w}| \to 0$.
Using Taylor once more, the linear approximation of the full system is now

$$\begin{aligned} \frac{\partial \bar{u}}{\partial t} &\approx \triangle \bar{u} + f_u(u_*, v_*)\bar{u} + f_v(u_*, v_*)\bar{v} \\ \frac{\partial \bar{v}}{\partial t} &\approx \varepsilon^2 \triangle \bar{v} + g_u(u_*, v_*)\bar{u} + g_v(u_*, v_*)\bar{v}. \end{aligned} \tag{33}$$

This can be written more compactly as

$$\mathbf{w}_t = d\triangle \mathbf{w} + J\mathbf{w}, \quad \text{with} \quad d = \begin{pmatrix} 1 & 0 \\ 0 & \epsilon^2 \end{pmatrix}. \tag{34}$$

A separation of variables leads to a time as well as a spatial variable;

$$\mathbf{w}(\mathbf{x}, t) = \psi(t)\phi(\mathbf{x})\mathbf{w}. \tag{35}$$

Inserting the expression (35) into (34) and dividing by $\psi(t)\phi(\mathbf{x})$ yields

$$\frac{\psi'(t)}{\psi(t)}\mathbf{w} = d\frac{\triangle\phi(\mathbf{x})}{\phi(\mathbf{x})}\mathbf{w} + J\mathbf{w}. \tag{36}$$

The left hand side of this equation is independent of space and the right hand side is independent of time. Therefore both the left hand and right hand side of (36) must be constant.
We set

$$\frac{\psi'(t)}{\psi(t)} = \lambda, \tag{37}$$

with $\psi(t) = \psi(0)e^{\lambda t}$ as before, and

$$\frac{\triangle\phi(\mathbf{x})}{\phi(\mathbf{x})} = -k^2, \quad \text{or } \triangle\phi(\mathbf{x}) = -k^2\phi(\mathbf{x}), \tag{38}$$

as J is also constant. Equation (38) is known as the *Helmholtz equation*. It is the eigenvalue problem for the Laplace operator. The generalised form is called *Sturm-Liouville problem* (Myint-U and Debnath 2007). Because the solution is a wave function, k is also known as the wavenumber. Function $\phi_k(\mathbf{x})$ is the eigenfunction corresponding to the wavenumber k. The problem is linear, therefore the solutions to the full system can be written as

$$\mathbf{w}(\mathbf{x}, t) = \sum_k c_k e^{\lambda t}\phi_k(\mathbf{x}). \tag{39}$$

The function $\phi_k(\mathbf{x})$ is still a function in two spatial dimensions. We perform another separation of variables for both spatial directions x and y,

$$\phi(x, y) = X(x)Y(y). \tag{40}$$

The zero flux boundary conditions from our Klausmeier model (4) can be converted to zero flux conditions for both dimensions separately. That way, the boundary conditions for $x \in \Omega$ and $y \in \Omega$ become

$$\left.\frac{\partial\phi(x)}{\partial n}\right|_{\partial\Omega} = 0 \quad \text{and} \quad \left.\frac{\partial\phi(y)}{\partial n}\right|_{\partial\Omega} = 0 \tag{41}$$

The definition of the two-dimensional Laplace operator replaces $\triangle$ in equation (38)

$$\triangle\phi(\mathbf{x}) + k^2\phi(\mathbf{x}) = \frac{\partial^2\phi}{\partial x^2}(\mathbf{x}) + \frac{\partial^2\phi}{\partial y^2}(\mathbf{x}) + k^2\phi(\mathbf{x}) = 0, \tag{42}$$

for $\mathbf{x} = (x, y)$ on domain

$$\Omega = \{(x, y) : \ 0 \leq x \leq p, \quad 0 \leq y \leq q\}. \tag{43}$$

We substitute (40) into (42) and divide by $X(x)Y(y)$ to derive

$$\frac{Y''(y)}{Y(y)} + k^2 = -\frac{X''(x)}{X(x)}. \tag{44}$$

Because the left hand side only depends on y and the right hand side only depends on x, both sides must be equal to a constant that we will denote μ. First we will solve the ODE for the x-direction

$$X''(x) + \mu X(x) = 0, \quad 0 \leq x \leq p, \tag{45}$$

with boundary conditions

$$X'(0) = X'(p) = 0. \tag{46}$$

For this one dimensional boundary value problem that it has now become, we find a solution

$$X(x) = a_1 cos(\sqrt{\mu}\ x) + a_2 sin(\sqrt{\mu}\ x). \tag{47}$$

Because of the zero flux boundary condition we have

$$X'(0) = -a_1\sqrt{\mu}\ sin(\sqrt{\mu}\ 0) + a_2\sqrt{\mu}\ cos(\sqrt{\mu}\ 0) = 0, \tag{48}$$

and therefore $a_2 = 0$, while

$$X'(p) = -a_1\sqrt{\mu}\ sin(\sqrt{\mu}\ p) = 0. \tag{49}$$

For $\mu > 0$, this gives a nontrivial solution $\sqrt{\mu}\ p = m\pi,$ for $m = 1, 2, ...$ and we are left with

$$X_m(x) = a_m cos\left(\frac{m\pi x}{p}\right), \quad \mu_m = \left(\frac{m\pi}{p}\right)^2, \quad m = 1, 2, 3, ... \tag{50}$$

Likewise, the problem

$$Y''(y) + \nu Y(y) = 0, \quad 0 \leq y \leq q, \tag{51}$$

with $\nu = (k^2 - \mu)$ and boundary conditions

$$Y'(0) = Y'(q) = 0, \tag{52}$$

has a similar solution

$$Y_n(y) = b_n cos\left(\frac{n\pi y}{q}\right), \quad \nu_n = \left(\frac{n\pi}{q}\right)^2, \quad n = 0, 1, 2, 3, ... \tag{53}$$

Hence, the eigenfunctions to the 2D Sturm-Liouville problem (38) are the functions

$$\phi_{m,n}(x, y) = X_m(x)Y_n(y) = c_{m,n} cos\left(\frac{m\pi x}{p}\right) cos\left(\frac{n\pi y}{q}\right), \quad m, n = 0, 1, 2, 3, ..., \tag{54}$$

which is a sequence of solutions, with eigenvalues

$$k^2 = \mu_m + \nu_n = \pi^2\left(\frac{m^2}{p^2} + \frac{n^2}{q^2}\right). \tag{55}$$

Any linear combination of the solutions with wavenumber k is again a solution to (6) with its boundary conditions (8).

$$u(x,y,t) = \sum_m \sum_n c_{m,n} e^{\lambda t} cos\left(\frac{m\pi x}{p}\right) cos\left(\frac{n\pi y}{q}\right), \quad m,n = 0,1,2,3,... \tag{56}$$

We will see in the next section how λ depends on m and n. We will not derive c_k in this thesis.
The stability of the model is is determined by the eigenvalues λ of the full system. These values now depend, not only on the Jacobian, but also on the values of wavenumber k. A compact way to describe the system is

$$\lambda \mathbf{w} = J\mathbf{w} - dk^2\mathbf{w}. \tag{57}$$

The two eigenvalues of the full system, λ_1 and λ_2 can be computed by solving the characteristic equation. In terms of f_u, f_v, g_u and g_v, the equation is

$$\lambda^2 - (k^2(1+\varepsilon^2) - (f_u + g_v))\lambda + h(k^2) = 0 \tag{58}$$

$$\text{with} \quad h(k^2) = \varepsilon^2 k^4 - (\varepsilon^2 f_u + g_v)k^2 + f_u g_v - f_v g_u. \tag{59}$$

2.3 Conditions for pattern formation

In order for patterns to develop, the system has to be (1) stable to heterogeneous perturbations and (2) unstable to spatial perturbations. But this is not sufficient, because some heterogeneous perturbations cause an instability that does not lead to a stable pattern (Doelman 2019). Therefore we need a homogeneous solution that is stable to homogeneous perturbations. Suppose we have a state as required, then we need one of the eigenvalues λ of the full system from equation (58) to be positive (see Table 1).
These eigenvalues λ depend on the wavenumber k. This is expressed in the so called *dispersion relation*

$$\lambda_{1,2}(k^2) = \frac{-(k^2(1+\varepsilon^2) - (f_u + g_v)) \pm \sqrt{(k^2(1+\varepsilon^2) - (f_u + g_v))^2 - 4h(k^2)}}{2}, \tag{60}$$

derived from (58) and (59).

The Klausmeier model

In case of the Klausmeier model, there are three equilibrium states, of which state B is unstable to homogeneous perturbations, and state A is the trivial stable state with no species v. Therefore we will restrict our analysis of the Klausmeier model to state C. The dispersion relation (60) of the full system in state C can be written as

$$\lambda^2 + (k^2(1+\varepsilon^2) + (1 + v_C^2 - m))\lambda + h(k^2) = 0$$
$$h(k^2) = \varepsilon^2 k^4 - (\varepsilon^2(-1 - v_C^2) - m)k^2 + (v_C^2 - 1)m. \tag{61}$$

We look for any $k > 0$ for which $\lambda(k^2) > 0$ that destabilises the system. Because of the condition on the trace, $(f_u + g_v) < 0$ (25), we know that the part $-(k^2(1+\varepsilon^2) - (f_u + g_v))$ is smaller than zero. Therefore the value of $h(k^2)$ must be smaller than zero. We have already established that the determinant of J should be positive (24) for linear stability of the homogeneous system. The only way $h(k^2)$ can be smaller than zero is when

$$\varepsilon^2 f_u + g_v > 0. \tag{62}$$

The trace of J had to be negative for the uniform steady state to be stable. Therefore f_u and g_v must have opposite sign and apart from $\varepsilon^2 \neq 1$, there are two cases

$$\begin{aligned} &\text{If} && f_u < 0 \text{ and } g_v > 0 \text{ then } \varepsilon^2 < 1 \\ &\text{and if} && f_u > 0 \text{ and } g_v < 0 \text{ then } \varepsilon^2 > 1. \end{aligned} \tag{63}$$

In the first case, u diffuses faster than v and in the second case v diffuses faster than u. They can not have the same diffusion coefficient, $\varepsilon^2 = 1$.
We need inequality (62) together with either one of the inequalities of (63) in order to have $\mathrm{Re}(\lambda) > 0$. But we also need the minimum value h_{min} to be negative. The point where $h(k^2) = 0$ is found by differentiating $h(k^2)$ with respect to k^2.

$$\begin{aligned} h(k^2) &= \varepsilon^2 k^4 - (\varepsilon^2 f_u + g_v)k^2 + (f_u g_v - f_v g_u) \\ \frac{dh}{dk_m^2} &= 2\varepsilon^2 k_m^2 - (\varepsilon^2 f_u + g_v) = 0 \\ k_c^2 &= \frac{\varepsilon^2 f_u + g_v}{2\varepsilon^2} \end{aligned} \tag{64}$$

Filling in the critical value of the wavenumber k_c^2 into $h(k^2)$ gives

$$\begin{aligned} h_{min}(k_c^2) &= \varepsilon^2 \frac{(\varepsilon^2 f_u + g_v)^2}{(2\varepsilon^2)^2} - \frac{(\varepsilon^2 f_u + g_v)^2}{2\varepsilon^2} + (f_u g_v - f_v g_u) \\ &= (f_u g_v - f_v g_u) - \frac{(\varepsilon^2 f_u + g_v)^2}{4\varepsilon^2}. \end{aligned} \tag{65}$$

For the inequality $h_{min} < 0$ needed to destabilise the system, we have found another condition for pattern formation

$$(\varepsilon^2 f_u + g_v)^2 - 4\varepsilon^2(f_u g_v - f_v g_u) > 0. \tag{66}$$

Setting (65) to zero and rewriting the expression to

$$\frac{f_u g_v - f_v g_u}{\varepsilon^2} = \left(\frac{\varepsilon^2 f_u + g_v}{2\varepsilon^2}\right)^2 \tag{67}$$

allows us to find another expression for k_c^2

$$k_c^2 = \frac{\varepsilon^2 f_u + g_v}{2\varepsilon^2} = \sqrt{\frac{f_u g_v - f_v g_u}{\varepsilon^2}}. \tag{68}$$

At the bifurcation point we can find the critical diffusion coefficient ε^2. We solve (65) set to zero for ε^2 and find

$$\varepsilon^2 = \frac{-(4f_v g_u - 2f_u g_v) \pm \sqrt{(4f_v g_u - 2f_u g_v)^2 - 4f_u^2 g_v^2}}{2f_u^2}. \tag{69}$$

The list of conditions necessary for patterns formation is now

$$\begin{array}{lll} 1. & f_u \text{ and } g_v \text{ must be of opposite sign} & \\ 2. & f_u + g_v < 0 & \text{(trace)} \\ 3. & f_u g_v - f_v g_u > 0 & \text{(determinant)} \\ 4. & \varepsilon^2 f_u + g_v > 0 \qquad \Rightarrow & \varepsilon^2 \neq 1 \\ 5. & (\varepsilon^2 f_u + g_v)^2 - 4\varepsilon^2(f_u g_v - f_v g_u) > 0. & \end{array} \tag{70}$$

2.4 Turing space

When parameter a becomes small enough, there will be a point where $h(k^2)$ changes sign. At that point the uniform steady state becomes unstable to non-uniform perturbations. After this bifurcation point Turing patterns can emerge. This change in stability is called a Turing bifurcation.
The conditions from (70) define a domain in parameter space. This domain is called pattern formation space or Turing space. (Murray 2003).

The Klausmeier model

To ensure the Klausmeier model has a Turing space, the conditions from (70) of the model in steady state C must be verified. First f_u and g_v must be of opposite sign. In case of the Klausmeier model, the Jacobian J is as follows;

$$J = \begin{pmatrix} f_u & f_v \\ g_u & g_v \end{pmatrix}_{(u_*,v_*)} = \begin{pmatrix} -(1+v^2) & -2uv \\ v^2 & -m+2uv \end{pmatrix}_{(u_*,v_*)} \tag{71}$$

The values of u and v must, because of their physical nature, be larger than zero. Because f_u is negative and g_u must be of opposite sign, it is clear that there can only be Turing patterns if $2uv > m$.
Computing the value of g_v at state C leads to the following inequality;

$$g_v|_{(u_*,v_*)} = -m + 2\left(\frac{2m^2}{a+\sqrt{a^2-4m^2}}\right)\left(\frac{a+\sqrt{a^2-4m^2}}{2m}\right) = -m + 2\frac{2m^2}{2m} = m > 0. \tag{72}$$

Parameter m can only have positive values, so the constraint that f_u and g_v must have opposite sign is met.
According to conditions 2 and 3, the trace of the Jacobian at C must be smaller than zero and the determinant must be larger than zero, as was proven in (25) and (24) respectively.
Because in the Klausmeier model $f_u < 0$ and $g_v > 0$, the fourth condition

$$\varepsilon^2 f_u + g_v = \varepsilon^2 m - 1 - v_C^2 > 0 \tag{73}$$

can only be true for $\varepsilon^2 < 1$, as stated in (63).
The final condition

$$(\varepsilon^2 f_u + g_v)^2 - 4\varepsilon^2(f_u g_v - f_v g_u) > 0 \tag{74}$$

can be reformulated into the inequality $\text{trace}^2(J) > 4\,\varepsilon^2$. This can be accomplished by changing parameter a for fixed values of m and ε^2 such that the requirement is met.
Figure 6 shows the homogeneous steady states of v as a function of bifurcation parameter a for fixed parameter value $m = 0,45$. When decreasing parameter a passes the Turing point, the solution is no longer stable to spatial perturbations.

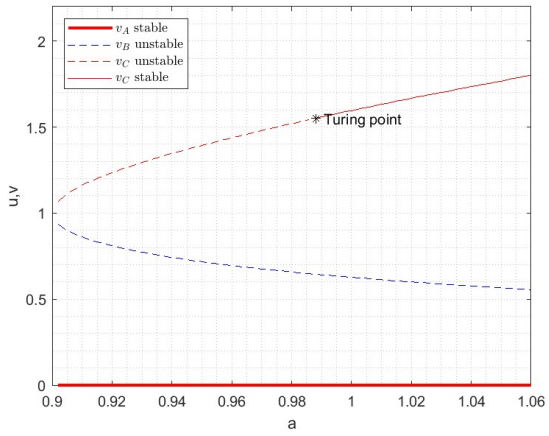

Figure 6: Turing point of the Klausmeier model for fixed values $m = 0.45$ and $\varepsilon^2 = 0.0108$. The value of v is plotted as a function of bifurcation parameter a. At the Turing point, conditions 4. and 5. from (70) no longer hold.

If $h(k^2) < 0$, then the full system has an eigenvalue larger than zero. In that case, possible wavenumbers can be obtained. Finite domains put restrictions on the number of allowable patterns, because the wavenumbers are discrete as can be seen from (55). For values of a smaller than the critical value a_c at the Turing point, fixed m and ε^2, an interval for positive wavenumber k^2 can be derived by solving $h(k^2) = 0$ (59) for k^2;

$$\begin{aligned} k_1^2 &= \frac{1}{2\varepsilon^2}[(\varepsilon^2 f_u + g_v) - \sqrt{(\varepsilon^2 f_u + g_v)^2 - 4\varepsilon^2 \det(J)}] < k^2 \\ &< \frac{1}{2\varepsilon^2}[(\varepsilon^2 f_u + g_v) + \sqrt{(\varepsilon^2 f_u + g_v)^2 + 4\varepsilon^2 \det(J)}] = k_2^2 \end{aligned} \tag{75}$$

If there are any wavenumbers k^2 within the range of unstable wavenumbers $[k_1^2, k_2^2]$, then a pattern will emerge. Only the patterns of these discrete wavenumbers will grow exponentially with time. Eventually they will be bounded by the nonlinear reaction terms of the system and stabilise into a nonhomogeneous steady state. (The study of a general perturbation analysis is not part of this thesis.)

The Klausmeier model

In Figure (7a) the effect of the bifurcation parameter a on the sign of function $h(k^2)$ is shown. For values of a larger than a_c, there are no negative values of $h(k^2)$, but for values smaller than a_c, part of the function $h(k^2)$ drops below the x-axis. In Figure (7b) the real part of the largest eigenvalue λ is plotted as a function of a. This value only becomes positive for values of a smaller than the Turing point.

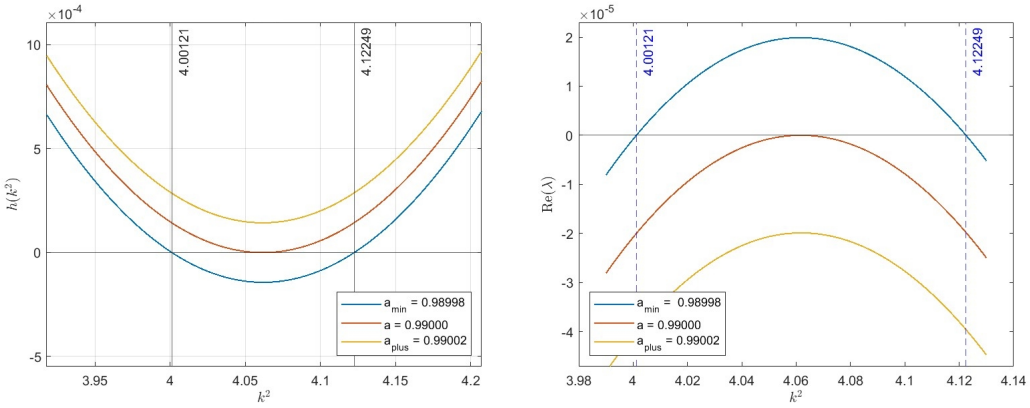

(a) Function $h(k^2)$ as function of k^2.

(b) Re(λ) as function of k^2

Figure 7: Two plots that show the effect of the value of parameter a on the stability of the Klausmeier model. Functions $h(k^2)$ and Re(λ) are plotted as functions of k^2 for parameter values $m = 0.45$, $a = 0.99$ and $d_c \approx 0.03896$.

2.5 Examples of solutions

On a bounded domain all wavenumbers must be discrete. Therefore it is possible that all conditions (70) are satisfied, and no patterns occur because there are no wavenumbers k^2 within the range of unstable wavenumbers $[k_1^2, k_2^2]$. According to (50) and (53), the zero flux boundary conditions only allow for solutions that are multiples of half a wavelength. Further away from the Turing point, when a is significantly smaller than at equilibrium, the interval (k_1^2, k_2^2) is larger and therefore potentially more wavenumbers fall inside the interval, hence more patterns can occur. But even when there are one or more wavenumbers in the interval, and all combinations of n and m are found, then numerical computations with eigenvalue solvers can still give different results. We give a specific example to show what to expect.

The Klausmeier model

For a domain that is $3\pi \times 4\pi$ and a critical wavelength $\omega = \pi$, the critical wavenumbers are $k_1^2 \approx 3.9267$ and $k_2^2 \approx 4.1979$. The wavenumbers for each combination of n and m can be computed with (55). Possible combinations of n and m are given in Table 2.

Table 2: Combinations of n and m and their wavenumber k^2.

n	m	k^2
6	0	4
6	1	4.0625
4	6	4.0778
3	7	4.0625
1	8	4.1111
0	8	4

A single combination like the one $(n, m) = (3, 7)$ is actually two patterns, because the mirror image about plane of the rest position of the waves is also an allowable solution.
That means that the negatives of Figure 8 are also allowed patterns.

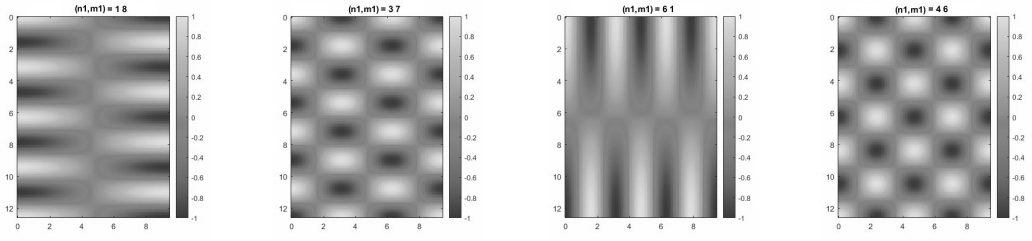

(a) $(n, m) = (1, 8)$ (b) $(n, m) = (3, 7)$ (c) $(n, m) = (6, 1)$ (d) $(n, m) = (4, 6)$

Figure 8: Four different combinations (m, n) for a domain of size $3\pi \times 4\pi$.

Apart from checkered patterns like the ones in Figure 8, sums of eigenvectors with identical wavenumbers can also be a solution and therefore a pattern. In Figure 9 the patterns in Figures 9a and 9b have identical wavenumbers (see Table 2). Their combination is the rhombus pattern in Figure 9c.
The eigenvector of the example in Figure 9c then becomes;

$$\begin{aligned} u(x, y, t) &= \sum_m \sum_n c_{m,n} e^{\lambda t} cos\left(\frac{m\pi x}{p}\right) cos\left(\frac{n\pi y}{q}\right), \quad m \in \{0, 8\}, n \in \{0, 6\} \\ &= c_{6,8} e^{\lambda t} \left(cos\left(\frac{6\pi y}{q}\right) + cos\left(\frac{8\pi x}{p}\right)\right) \end{aligned} \tag{76}$$

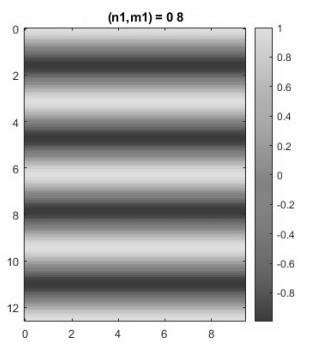

(a) $(n1, m1) = (0, 8)$

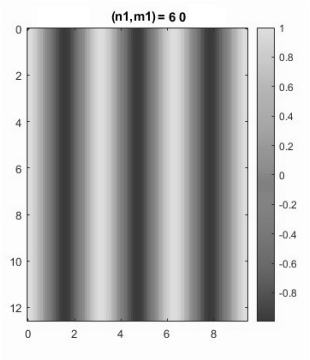

(b) $(n2, m2) = (6, 0)$

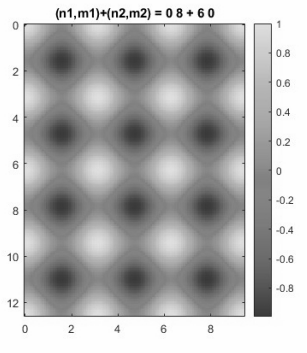

(c) $(n1, m1) + (n1, m1) = (0, 8) + (6, 0)$

Figure 9: Two different patterns, $(n1, m1) = (0, 8)$ and $(n2, m2) = (6, 0)$ with identical wavenumber k^2 and their sum $(n1, m1) + (n1, m1) = (0, 8) + (6, 0)$

3 Methods

We will investigate the effects of the Klausmeier model working on a sequence of networks that gradually change from a regular rectangular lattice to a random network. Each network differs from the previous one by a small change of two edges. The analytical solution from Section 2.2 is only available for regular domains, like a rectangular one for example. As soon as the domain starts to deform, it will no longer be certain that an analytical solution can be found. But if we replace the continuous domain by a discrete version, a discrete solution can be obtained numerically. First we will discretise the system and analyse the stability against homogeneous and non-homogeneous perturbations. The section after that will be a detailed description of how the regular lattice will be transformed into a random network by altering the discrete Laplacian in every step. This will provide us with a method to investigate the stability of both the regular lattice as well as the deforming network.

3.1 Analysis of the model on a fixed lattice

The starting point is the simplest discretisation of a rectangular domain, namely a fixed rectangular lattice. Let $\Omega := [0, l] \times [0, m]$ be the continuous domain of the differential equation (9). We discretise the domain into a regular lattice that has $p+1$ points horizontally and $q+1$ points vertically with an equal step size h in both directions.
The following relations apply to the discretisation;

$$l = (p-1)h, \; m = (q-1)h \quad \text{for certain } p, q \in \mathbb{N}. \tag{77}$$

We define the inner points of the lattice, which are the black dots in Figure 10a, as

$$\Omega_h \quad := \quad \{x_{i,j} | i = 2, ..., p-1, j = 2, ..., q-1\}, \tag{78}$$

and boundary points of the lattice, the open circles in Figure 10a, as;

$$\delta\Omega_h \quad := \quad \{x(i,j) | i \in \{1, p\}, j \in \{1, ..., q\} \text{ or } i \in \{1, ..., p\}, j \in \{1, q\}\} \tag{79}$$

The approximation of the differential equation has to be satisfied on all of these points. The set of all grid points is defined as

$$\overline{\Omega}_h := \Omega_h + \delta\Omega_h \tag{80}$$

In order to make a the numerical computations, the lattice needs to be vectorised. To do so, all vertices are numbered from bottom left to upper right corner like in Figure 10b. Both species must be represented, therefore the vector will be twice the number of grid points of the domain. For the two-dimensional domain the vector is defined as

$$\begin{pmatrix} u \\ v \end{pmatrix}(x,t) \quad \rightarrow \quad \begin{pmatrix} u(x_1,t) \\ u(x_2,t) \\ ,, \\ ,, \\ u(x_n,t) \\ v(x_1,t) \\ v(x_2,t) \\ ,, \\ ,, \\ v(x_n,t) \end{pmatrix} = \begin{pmatrix} y_u \\ y_v \end{pmatrix} \tag{81}$$

The vector describes the amount of water and vegetation on each grid point on the discretised domain $\overline{\Omega}_h$.

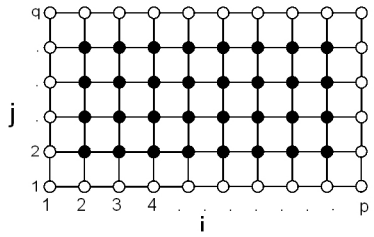

(a) Two-dimensional grid where the filled circles represent the discrete set of points Ω_h, and the open circles represent the set of boundary points $\delta\Omega_h$. In this figure, $p = 10$ and $q = 6$.

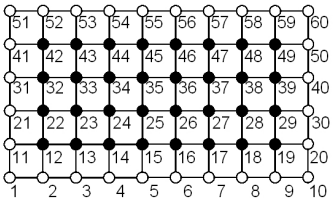

(b) The vertices x_n, $n = 1, 2, ..., N$ of the network are ordered from bottom left corner to upper right corner.

Figure 10: Discretisation scheme for the transformation from continuous domain Ω to lattice $\overline{\Omega}_h$ and from lattice $\overline{\Omega}_h$ to vectors y_u and y_v.

The next step is to replace the continuous Laplace operator $\triangle$ by a discrete version; the discrete Laplacian matrix L. For the discretisation we use the finite difference method (Knabner and Angermann 2021) and the five-point stencil (see Figure 11).

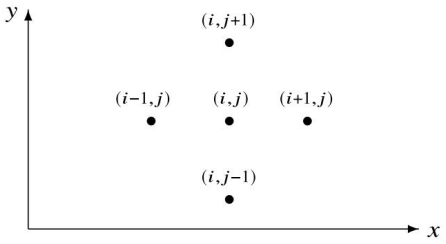

Figure 11: The five-point stencil.

On a two dimensional lattice, the discrete Laplacian matrix L for the approximation of the second order spatial derivative is now a $pq \times pq$ matrix that is build up out of different types of block matrices. All these block matrices have size $p \times p$ and there are $q \times q$ block matrices in total.
The block matrices L_D (83) are on the diagonal of L and on the superdiagonal and subdiagonal are identity matrices I, or $2I$ in case of boundary conditions (82).
The discrete Laplacian matrix L looks like;

$$L = \frac{1}{h^2}\begin{pmatrix} L_D & 2I & & & & \\ I & L_D & I & & \emptyset & \\ & \cdot & \cdot & \cdot & & \\ & & \cdot & \cdot & \cdot & \\ & \emptyset & & I & L_D & I \\ & & & & 2I & L_D \end{pmatrix} \tag{82}$$

with

$$L_D = \begin{pmatrix} -4 & 2 & & & & \\ 1 & -4 & 1 & & \emptyset & \\ & \cdot & \cdot & \cdot & & \\ & & \cdot & \cdot & \cdot & \\ & \emptyset & & 1 & -4 & 1 \\ & & & & 2 & -4 \end{pmatrix}, \text{ and } \qquad I = \begin{pmatrix} 1 & & & & \\ & 1 & & \emptyset & \\ & & \cdot & & \\ & & & \cdot & \\ & \emptyset & & 1 & \\ & & & & 1 \end{pmatrix} \tag{83}$$

With this definition of L, we can write the system of reaction diffusion equations (6) in vector form

$$\frac{d}{dt}\begin{pmatrix} y_u \\ y_v \end{pmatrix} = \begin{pmatrix} Ly_u \\ \varepsilon^2 Ly_v \end{pmatrix} + \begin{pmatrix} \bar{f}(y_u, y_v)) \\ \bar{g}(y_u, y_v)), \end{pmatrix}, \tag{84}$$

where $\bar{f}(y_u, y_v)$ and $\bar{g}(y_u, y_v)$ represent the reaction equations $f(u(x_k), v(x_k))$ and $g(u(x_k), v(x_k)) : \mathbb{R}^2 \to \mathbb{R}^2$ at all points $(x_k),\ k = 1, 2, ..., pq$ in the discrete domain.
Suppose, like in the continuous case in Section 2.2.1, this discretised system has a uniform steady state

$$\begin{pmatrix} y_{u_*} \\ y_{v_*} \end{pmatrix}, \text{ with } \quad y_{u_*} = u_* \begin{pmatrix} 1 \\ \vdots \\ 1 \end{pmatrix}, \text{and} \quad y_{v_*} = v_* \begin{pmatrix} 1 \\ \vdots \\ 1 \end{pmatrix}. \tag{85}$$

We will use the remainder of this section to show how we can determine the linear stability of any homogeneous steady state of the discrete system. Therefore we define a perturbation

$$\begin{pmatrix} \bar{y}_u \\ \bar{y}_v \end{pmatrix} = \begin{pmatrix} y_u - y_{u_*} \\ y_v - y_{v_*} \end{pmatrix}, \tag{86}$$

with $\left| \begin{pmatrix} \bar{y}_u \\ \bar{y}_v \end{pmatrix} \right|$ small.
Linearising around steady state like in the continuous case (14), we define Jacobian matrix J_d

$$J_d = \begin{pmatrix} f_u & & & & f_v & & & \\ & \ddots & & & & \ddots & & \\ & & \ddots & & & & \ddots & \\ & & & \ddots & & & & \ddots \\ & & & f_u & & & & f_v \\ g_u & & & & g_v & & & \\ & \ddots & & & & \ddots & & \\ & & \ddots & & & & \ddots & \\ & & & \ddots & & & & \ddots \\ & & & g_u & & & & g_v \end{pmatrix} \begin{pmatrix} y_{u_*} \\ y_{v_*} \end{pmatrix}, \tag{87}$$

evaluated at the steady state.
Equation (84) can now be written as

$$\frac{d}{dt} \begin{pmatrix} \bar{y}_u \\ \bar{y}_v \end{pmatrix} = D \begin{pmatrix} \bar{y}_u \\ \bar{y}_v \end{pmatrix} + J_d \begin{pmatrix} \bar{y}_u \\ \bar{y}_v \end{pmatrix}, \text{ where } \quad D = \begin{pmatrix} L & 0 \\ 0 & \varepsilon^2 L \end{pmatrix}. \tag{88}$$

By separation of variables, the time component can be taken out of vector $\begin{pmatrix} \bar{y}_u \\ \bar{y}_v \end{pmatrix}$. The space component is embedded in the location inside the remaining part of $\begin{pmatrix} \bar{y}_u \\ \bar{y}_v \end{pmatrix}$, which will be denoted by χ with subscript $i = 1, 2, ...n$ for all n points on the grid.

$$\begin{pmatrix} \bar{y}_u \\ \bar{y}_v \end{pmatrix}(t) = T(t) \begin{pmatrix} \chi_1 w_1 \\ \vdots \\ \chi_n w_1 \\ \chi_1 w_2 \\ \vdots \\ \chi_n w_2 \end{pmatrix} \tag{89}$$

This expression can be written in a more compact way by defining;

$$X = \begin{pmatrix} \chi_1 \\ \chi_2 \\ \vdots \\ \chi_n \end{pmatrix}, \text{ such that } \quad \overline{\chi w} = \begin{pmatrix} X w_1 \\ X w_2 \end{pmatrix}, \tag{90}$$

which leads to the expression

$$\begin{pmatrix} \bar{y}_u \\ \bar{y}_v \end{pmatrix}(t) = T(t) \begin{pmatrix} X(x)w_1 \\ X(x)w_2 \end{pmatrix}. \tag{91}$$

Substituting (91) into (88) leads to the following equation;

$$\frac{T'(t)}{T(t)} \begin{pmatrix} X(x)w_1 \\ X(x)w_2 \end{pmatrix} = D \begin{pmatrix} X(x)w_1 \\ X(x)w_2 \end{pmatrix} + J_d \begin{pmatrix} X(x)w_1 \\ X(x)w_2 \end{pmatrix}. \tag{92}$$

Only the left hand side is time dependent, therefore for any solution $\frac{T'(t)}{T(t)}$ must be constant. Like in the continuous case, we can substitute Ansatz $T(t) = T(0)e^{\lambda t}$ into equation (92) and derive the eigenvalue problem;

$$\lambda \overline{\chi w} = (D + J_d)\overline{\chi w}. \tag{93}$$

The solution to the discrete system must be of the form;

$$\begin{pmatrix} \bar{y}_u \\ \bar{y}_v \end{pmatrix}(t) = \sum_j c_j \overrightarrow{v_j} e^{\lambda_j t}, \tag{94}$$

where λ_j, $\overrightarrow{v_j}$ forms an eigenvalue, eigenvector pair for the matrix $(D + J_d)$.

At least one of the eigenvalues of matrix $(D + J_d)$ must be larger than zero in order for the system to be unstable to spatial perturbations and develop patterns. In the continuous case the eigenvalues λ depended on the wavenumber k^2, while here the eigenvalues λ depend on the eigenvalues μ of the discrete Laplacian L.

3.2 Changing the lattice to a random network

The main focus of this thesis is to investigate what happens to the destabilised eigenfunctions of reaction-diffusion equations if the network on which the equations are posed becomes increasingly less regular. By discretising the reaction diffusion equation from working on a continuous rectangular domain to working on a rectangular lattice in the previous section, we have derived a method that can be applied to any network. The lattice needs to become less regular in small steps in order to 'follow' the destabilising eigenvalues and their eigenfunctions. We will study their behavior as the network changes. In this section we describe the process that is used to gradually randomise the regular lattice. After that we will see that the discrete Laplacian in the case of our regular lattice, is not so different from its graph Laplacian.

3.2.1 Randomisation of the network

To investigate the effect of reaction diffusion equations on a network, the regular lattice will be slowly transformed into a slightly more random network. We define a *swap* as performing the following procedure: randomly choose two edges (Figure 12a), delete them and reconnect the vertices on either side of the edge to a vertex belonging to the other edge (Figure 12b). By performing a large number of swaps, the network will eventually become random. We want the number of vertices and edges, as well as the degree of the network to stay the same. Also the boundary conditions need to be considered. Therefore we describe a procedure for choosing the edges and reconnecting the vertices.
All the information of the lattice is stored inside the discrete Laplacian. An edge between vertex i and j is also an edge between vertex j and i. That makes matrix L almost symmetric, except for entries that represent a boundary condition. These entries have a value of $2/h^2$. We only need to consider the upper triangular part of the matrix to find any edge of the lattice. Every entry in the upper triangular part of L represents an edge. When choosing an entry in the upper triangular part, the entry itself, as well as its mirror image in lower triangular part must be checked for boundary conditions.
There are two sets of vertices and therefore there are two different ways to reconnect the vertices. Since both vertices are chosen from the upper triangular part of the discrete Laplacian matrix, it makes sense

to reconnect the vertices in the way that is shown in Figure 13, where horizontal and vertical lines are drawn to determine the location of the new edges at the point where these lines meet. Since the discrete Laplacian is symmetric, apart from the boundary conditions, entries mirrored in the diagonal must be adjusted in the same manner.
There are a couple of constraints for the swap;

1. the swap will not affect the boundary conditions,
2. no double edges will appear,
3. there is a maximum distance that the edges that are deleted can be apart.

To see how these conditions are implemented, the discrete Laplace matrix L is quite useful. Figure 13 shows a random swap in a small network. The entries inside the red circles are the edges that are being swapped. There are four entries encircled because of the symmetry of matrix L around the diagonal for non boundary points. These four entries with value 1 will become zero. Four other entries with value zero inside the red boxes will become one. That way the total row sum will remain zero, which means that the matrix will always have one eigenvalue zero, and the boundary conditions will remain intact, although they may no longer have a meaning in a deformed lattice.

The way these rules are implemented are as follows;
1. If we ignore the factor $1/h^2$, the boundary conditions are reflected by the entries with value two in matrix L. Their counterpart, or mirror image, on the other side of the diagonal, is not two, but one. Both entries are taken into account when deciding whether a swap can be performed, and if one of the two mirror images is 2, the choice is rejected.
2. To prevent double edges from being created, the entry in which the new edge will be placed must be zero. All zeros in matrix L are symmetric around the diagonal.
3. Bounding the distance between two chosen edges means that the new entries of the discrete Laplace matrix stay close to the diagonal. Since L is a very large matrix ($nx \times ny \times 2$ by $nx \times ny \times 2$) and tri-diagonal with two off diagonals at distance ny, it will take a very large number of swaps for nonzero entries to reach the top right and bottom left of the matrix. In Section 4.3.2 this is treated in detail. Because of this effect, it is useful to keep track of the distance between the swapped edges. The maximum distance between a single vertex at one end of the first edge and a single vertex at one edge of the second edge in the x and y direction is five edges. This is an arbitrary choice. Smaller steps make the randomising of the network take longer. Allowing for larger steps will speed up the randomisation, but also make the changes in the process more difficult to interpret. In Section 4.3.5 it will become clear why this is important.
For edges that exist in the initial rectangular lattice, the absolute maximum distance between the center of the two edges is at most $\sqrt{(5.5h)^2 + (5.5h)^2} \approx 7.78h$. Once edges that have already been swapped are involved in a second swap, the computed distance will depend on the vertex that is chosen. This means that the distance between the centre of two swapped edges can eventually become larger. An example of such a second generation swap is given in Figure 12, where the average distance between the two edges is $\sqrt{(7h)^2 + (4.5h)^2} \approx 8.32h$. The expectation is that this will most likely speed up the process.

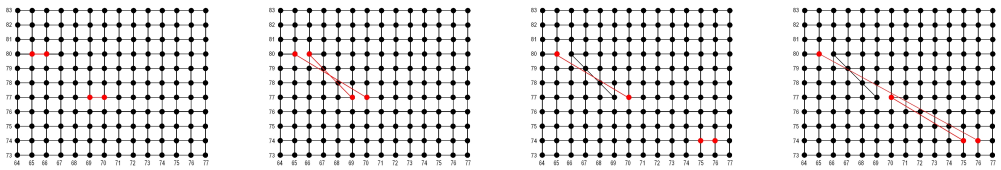

(a) Regular lattice without edge swap.

(b) Lattice with the first edge swap.

(c) Choosing two new edges for a swap, one of which was formed in the previous swap.

(d) Lattice after the second swap.

Figure 12: Two random edges between two different sets of vertices are randomly chosen (a) and deleted. Then two different edges connecting two different sets of the same four vertices are created (b). After choosing two edges, one of which was formed in the previous swap (c), vertices are connected over a greater distance (d).

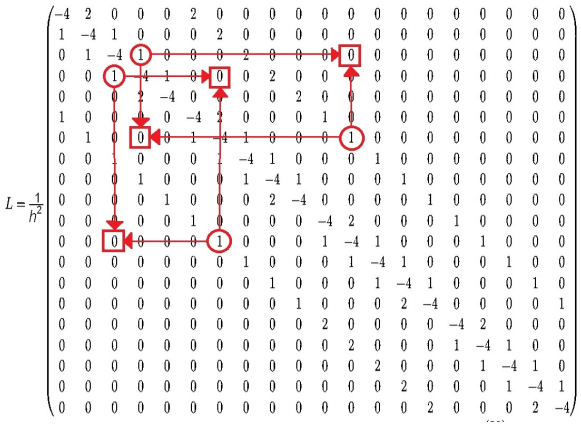

Figure 13: Example of a swap on a graph Laplacian. Two chosen edges are being deleted (red circles) and two new edges are created (red squares).

It seems very unlikely that the network will become unconnected during the swapping procedure. However,the possibility is also not completely ruled out, and we did not encounter it during the procedure.

3.2.2 The graph Laplacian

So far we have seen the Laplacian operator Δ and its lattice equivalent the discrete Laplacian matrix L. The lattice itself is a network and therefore has a graph Laplacian. Because of the boundary conditions on our model, these two Laplacian matrices are not the same.
A graph Laplacian is defined as follows; Let G be an undirected network consisting of N ordered vertices $i \in 1, 2, 3, ..., N$. Define an adjacency matrix A as

$$A_{i,j} = \begin{cases} 1\ , & \text{if there is a connection between vertex } i \text{ and vertex } j,\ i \neq j, \\ 0\ , & \text{otherwise} \end{cases} \tag{95}$$

Define the diagonal matrix D with $D_{i,i} = d_i$, d_i being the degree of vertex i.
Then the graph Laplacian GL is defined as,

$$GL = A - D, \tag{96}$$

and

$$GL_{i,j} = \begin{cases} \text{degree vertex}(i) & \text{if } i = j \\ -1 & \text{if } i \neq j \text{ and } vertex(i) \text{ is adjacent to } vertex(j) \\ 0 & \text{otherwise .} \end{cases} \tag{97}$$

One of the properties of a graph Laplacian is that all rows as well as all columns add up to zero. An example of a lattice is given in Figure 14. Its graph Laplacian matrix GL is given in Figure (98).

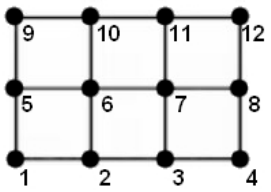

Figure 14: Example of a lattice *Made in Paint and PhotoFiltre*.

The graph Laplacian GL in this case is as follows

$$GL = \begin{pmatrix} -2 & 1 & 0 & 0 & 1 & 0 & 0 & 0 & 0 & 0 & 0 & 0 \\ 1 & -3 & 1 & 0 & 0 & 1 & 0 & 0 & 0 & 0 & 0 & 0 \\ 0 & 1 & -3 & 1 & 0 & 0 & 1 & 0 & 0 & 0 & 0 & 0 \\ 0 & 0 & 1 & -2 & 0 & 0 & 0 & 1 & 0 & 0 & 0 & 0 \\ 0 & 0 & 0 & 0 & -3 & 1 & 0 & 0 & 1 & 0 & 0 & 0 \\ 1 & 0 & 0 & 0 & 1 & -4 & 1 & 0 & 0 & 1 & 0 & 0 \\ 0 & 1 & 0 & 0 & 0 & 1 & -4 & 1 & 0 & 0 & 1 & 0 \\ 0 & 0 & 1 & 0 & 0 & 0 & 1 & -3 & 0 & 0 & 0 & 1 \\ 0 & 0 & 0 & 1 & 0 & 0 & 0 & 0 & -2 & 1 & 0 & 0 \\ 0 & 0 & 0 & 0 & 1 & 0 & 0 & 0 & 1 & -3 & 1 & 0 \\ 0 & 0 & 0 & 0 & 0 & 1 & 0 & 0 & 0 & 1 & -3 & 1 \\ 0 & 0 & 0 & 0 & 0 & 0 & 1 & 0 & 0 & 0 & 1 & -3 \end{pmatrix} \tag{98}$$

The discrete Laplacian of the same lattice, now with zero flux boundary conditions is derived as in (82) and (83)

$$L = \frac{1}{h^2} \begin{pmatrix} -4 & 2 & 0 & 0 & 2 & 0 & 0 & 0 & 0 & 0 & 0 & 0 \\ 1 & -4 & 1 & 0 & 0 & 2 & 0 & 0 & 0 & 0 & 0 & 0 \\ 0 & 1 & -4 & 1 & 0 & 0 & 2 & 0 & 0 & 0 & 0 & 0 \\ 0 & 0 & 2 & -4 & 0 & 0 & 0 & 2 & 0 & 0 & 0 & 0 \\ 0 & 0 & 0 & 0 & -4 & 2 & 0 & 0 & 1 & 0 & 0 & 0 \\ 1 & 0 & 0 & 0 & 1 & -4 & 1 & 0 & 0 & 1 & 0 & 0 \\ 0 & 1 & 0 & 0 & 0 & 1 & -4 & 1 & 0 & 0 & 1 & 0 \\ 0 & 0 & 1 & 0 & 0 & 0 & 2 & -4 & 0 & 0 & 0 & 1 \\ 0 & 0 & 0 & 2 & 0 & 0 & 0 & 0 & -4 & 2 & 0 & 0 \\ 0 & 0 & 0 & 0 & 2 & 0 & 0 & 0 & 1 & -4 & 1 & 0 \\ 0 & 0 & 0 & 0 & 0 & 2 & 0 & 0 & 0 & 1 & -4 & 1 \\ 0 & 0 & 0 & 0 & 0 & 0 & 2 & 0 & 0 & 0 & 2 & -4 \end{pmatrix} . \tag{99}$$

We have now developed a procedure to gradually change the network, as well as a method to determine the stability of the homogeneous state. In the next section we explore how the eigenfunction/eigenvalue solutions change as the network changes. By lattice, the initial unperturbed discretised domain is indicated, and by network the domain after one or more swaps have been performed. To distinguish

the networks during the process, we will use 'swap' in combination with a number indicating the number of swaps that has been performed so far. In the next section the discrete Laplacian matrix, as defined in (82) and (83), and not the graph Laplacian, represents the network.
The model runs in the following section were performed in MATLAB (version 2023b, The MathWorks, Inc.). For any numerical simulations the Matlab ODE ode15s was used.

4 Results

Before analysing the stability of the discretised reaction diffusion equations on the network, we will first analyse the continuous system on a rectangular domain of fixed size. In the continuous case, we will use the the linearised system to find the destabilisation that led to the eigenvalue problem in equations (22) and (93).
By solving the system both analytically on the continuous domain as well as numerically on the initial lattice, we can compare all possible solutions. Thus we know how trustworthy our numerically derived solutions are in case the network becomes too random to find solutions analytically. A third way to verify the results is by performing numerical simulations. These solutions are very sensitive to initial conditions, as we will see in Section 4.2.
The derivation of the destabilised eigenfunctions and eigenvectors for the initial fixed domain will be the starting point of the experiment. Once the initial unstable eigenfunctions and eigenvalues are derived, the lattice will be changed by swaps defined as in Section 3.2.1. We will explore how the eigenvalues-eigenvector solutions change during the course of the process as the network becomes more random.

4.1 The initial fixed rectangular domain

We set the parameters of the reaction part of the equations to $m = 0.45$ and $a = 0.99$. With these values fixed, the critical diffusion can be computed with equation (69). At a critical diffusion value of $\varepsilon_c^2 \approx 0.039$ the system is precisely at the Turing point. According to the theory, for the homogeneous solution to destabilise, the bifurcation parameter a needs to be smaller than the critical value $a_c = 0.99$. As can be seen in Figure 7a, for $a = 0.98998$ there is indeed an interval (k_1^2, k_2^2) where $Re(\lambda) > 0$. The eigenfunctions (54) that are linearly unstable are selected if and only if they have a wavenumber k such that $k_1^2 < k^2 < k_2^2$.
Using equation (75), the boundaries of the interval for a domain of size $p \times q = 2.81\pi \times 4.34\pi$ yield

$$\begin{aligned} k_1^2 &\approx 4.0012 \\ k_2^2 &\approx 4.1225. \end{aligned} \tag{100}$$

The wavenumbers for each combination of n and m can be computed with (55). In this specific case, there is only one possible combination of n and m that yields a positive eigenvalue λ (see Table 3).

Table 3: The single combination of n and m and their wavenumber k^2 for domain size $p = 2.81\pi$ and $q = 4.34\pi$.

n	m	k^2
5	4	4.0156

The number of discretisation points of the domain is set at $nx = 100$ and $ny = 154$. Because we also want to compare the analytical and the discrete solution to the solution of a numerical simulations, the number of points can not be too large. Otherwise the Matlab program ode15s will run out of memory while trying to find a solution.
We find one unstable eigenfunction with both the analytical approach and the numerical approximation. The analytical eigenfunction can easily be plotted. It is already defined on a two dimensional domain because it depends on x and y. The discrete solution however, is a one dimensional eigenvector that has to be transformed to the rectangular lattice before it can be visually compared to the analytical solution. The analytically derived eigenfunction in Figure 15a, and numerical derived eigenvector in Figure 15b are out of phase, but do otherwise align. We can conclude that in the case the analytic solutions are not available, we can rely on the numerical computations.

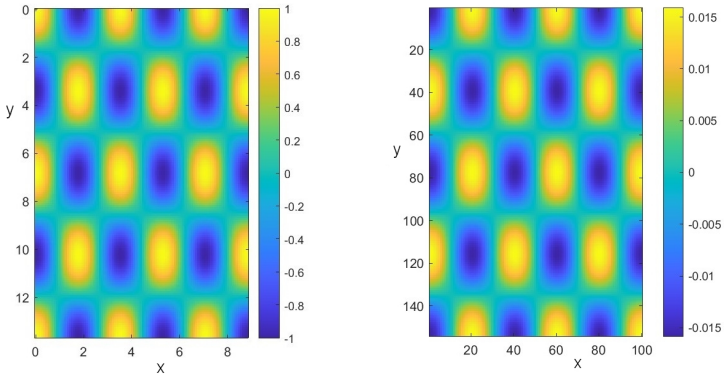

(a) The unstable eigenfunction found with the analytical approach.

(b) The unstable eigenfunction found by the numerical approximation.

Figure 15: The analytically found unstable eigenfunction (a) compared to the numerically derived unstable eigenvector (b) on the domain of size $2.81\pi \times 4.34\pi$ with a fixed diffusion coefficient $\varepsilon_c^2 \approx 0.039$ and a fixed parameter $a = 0,98998$. The analytical approach and the numerical approximation align, apart from being out of phase.

4.2 Numerical simulations

In this section we study the results of a numerical time integration of the model. We use the same parameter values as in the previous section as well as the discretised domain we defined for the numerical approximation. Using the discretisation of the Laplace operator, the system of partial differential equations becomes an ODE that can be solved with the Matlab ODE ode15s. The initial condition of the system is vector $y_0 = (y_{u_0} y_{\tilde{v}_0})^T$, where u_0 is the vector $u_*(1...1)^T$. The vector $\tilde{v}_0$ is the vector $v_0 = v_*(1...1)^T$ after perturbation by uniformly distributed random noise with a small amplitude of $\sigma = 0.00001$. During the integration, parameter a is decreased stepwise, starting at the Turing point $a = 0.99$ until the end value of $a = 0.98996$ is reached. The system will pass the value $a = 0.98998$ where the destabilising patterns from Figure 15 were found. We have run the numerical simulations 40 times. The solutions of five simulations with each a different initial condition are plotted in Figure 16. As can be seen, only the the pattern in Figure 16c resembles the initial analytical and discrete unstable eigenfunction. The other patterns in Figure 16 are eigenfunctions or sums of eigenfunctions that can be found analytically and numerically for different parameter values.

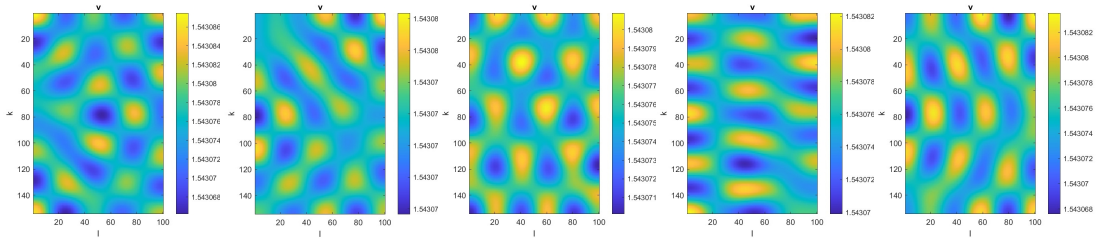

(a) (b) (c) (d) (e)

Figure 16: The results of five numerical simulations with different initial conditions.

Obviously the unstable eigenvectors of the numerical simulations are very sensitive to initial conditions.

4.3 Network experiment

The actual experiment is the creation of a progressively randomising sequence of networks. We determine the stability of the reaction diffusion equation posed on the networks and study the destabilising eigenvector-eigenvalue solutions. First we will examine the effects of the swaps on the network itself and on its properties. Then we will study the result of the edge swaps on the discrete Laplacian and its eigenvalues. This will allow us to determine the relation between the eigenvalues of the discrete Laplacian and the eigenvalues of the full system. The patterns and the order in which they appear as the network slowly becomes less regular, can be explained by this relation, which we will derive in Section 4.3.3.

4.3.1 Change of the network

In this section we will examine the changes to the three-dimensional network and its properties resulting from the swaps. The starting point for the network experiment will be the parameter values that were used in Section 4.1. That means that the initial domain size is $2.81\pi \times 4.34\pi$. The number of vertices in the horizontal and vertical direction are $nx = 100$ and $ny = 154$ respectively and therefore the network consists of a total of 15400 vertices.
On this domain two edges are broken and their vertices reconnected in the manner described in Section 3.2.1. At swap 5, five swaps have been performed. The result over the first 9000 swaps is visualised in Figure 17. Compared to the projections on the initial lattice, these networks are rotated 90° counterclockwise. Although the lattice structure of the original network after 9000 swaps is no longer visible, the global shape is still rectangular. The reason for this is that the distance between the pairs of swapped edges is relatively small compared to the size of the network.

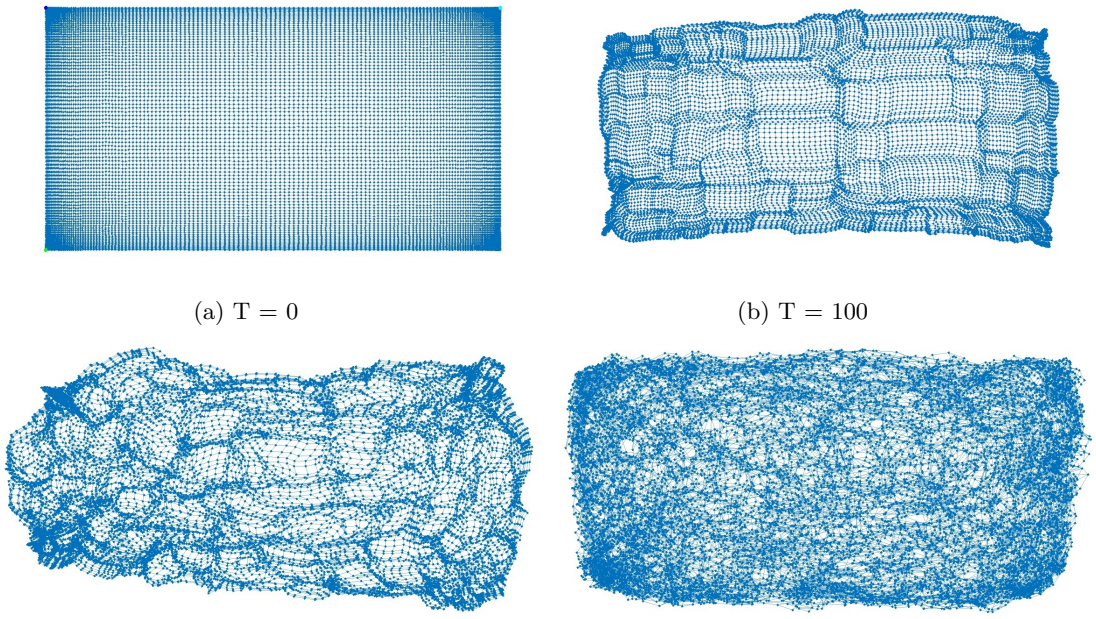

(a) T = 0 (b) T = 100

(c) T = 1000 (d) T = 9000

Figure 17: The deformation of the network at zero, 100, 1000 and 9000 swaps.

The number of edges in the lattice is 30546. Some of these edges have boundary condition on them and are excluded from the swap procedure, so the total number of edges to choose from is 30038.
In each time step, two edges are deleted (=0.0066 %) and two new ones are formed. Some of these deleted edges may have been created in a previous swap, but a rough estimate of the change of the

lattice after 9000 swaps is that $(2 * 9000)/30038 * 100 \approx 60\%$ of the edges has been swapped.
During the swapping procedure, the total number of vertices and edges does not change. Also the degree of any node stays the same. There are other properties of the network that do change;

1. the *distance* between vertices, which is number of edges in a shortest or minimal path between two vertices,

2. the *eccentricity* of the vertices, which is the maximum distance of one vertex from all other vertices.

The change of the eccentricity affects the *radius* and *diameter* of the network which are defined as the minimum and maximum eccentricity respectively. The *center* is the number of vertices that have minimum eccentricity.
In Figure 18a, the diameter, radius and center of the network are plotted in every swap step for the first 700 steps. As predicted, the diameter and the radius decrease rapidly, but as more original edges disappear, swapping will no longer guarantee that a shorter path is created. It may even occur that a swap increases the diameter. At swap 146, diameter as well as radius increase in size, and at swap 254 the diameter increases. After 700 swaps, the values of the properties are only measured once per 1000 swap steps. The plot in Figure 18b shows that the decrease of the diameter and the radius continues, but slows down even further.

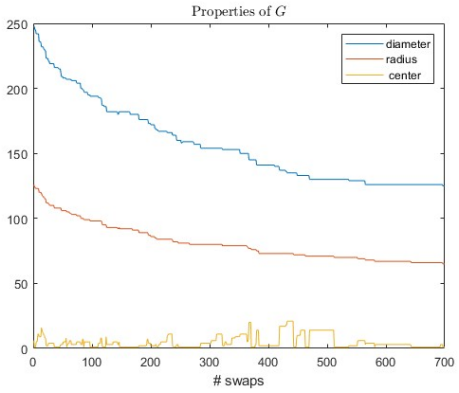

(a) Properties of the first 700 swaps.

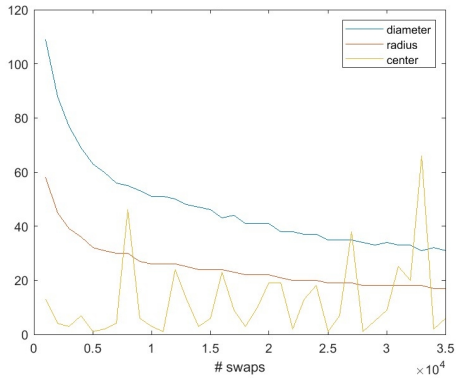

(b) Properties per 1000 swaps from swap 1000 to swap 35000.

Figure 18: The change of the three network properties diameter, radius and center over time for the first 700 swaps (a), and for swap 1000 up to swap 35000, sampled once per 1000 swaps (b) *Matlab*.

The number of nodes with equal radius, the center, does fluctuate over time but there is no trend of it increasing or decreasing.

4.3.2 Change of the discrete Laplacian

In Section 3.2 the significance of the structure of the network for the discrete Laplace operator L was shown. The structure of the network determines the structure of L, so if the network changes, then so does the discrete Laplacian. This happens in a very orderly way. At the beginning of the experiment, matrix L only has nonzero entries in the main diagonal, the 1^{st} and nx^{th} superdiagonals and subdiagonals. Following the method described in that same section, the new entry will be on a diagonal that is at most at distance $6nx$ from the diagonal. For the 15400×15400 discrete Laplacian this distance is 600. It will take a very large amount of swaps for nonzero entries to reach the top right and bottom left entries of the matrix. Figure 19 shows the upper left quarter of the matrix L at four different stages of randomisation. The number of entries stays the same but the number of entries that are not on the initial five diagonals increases.

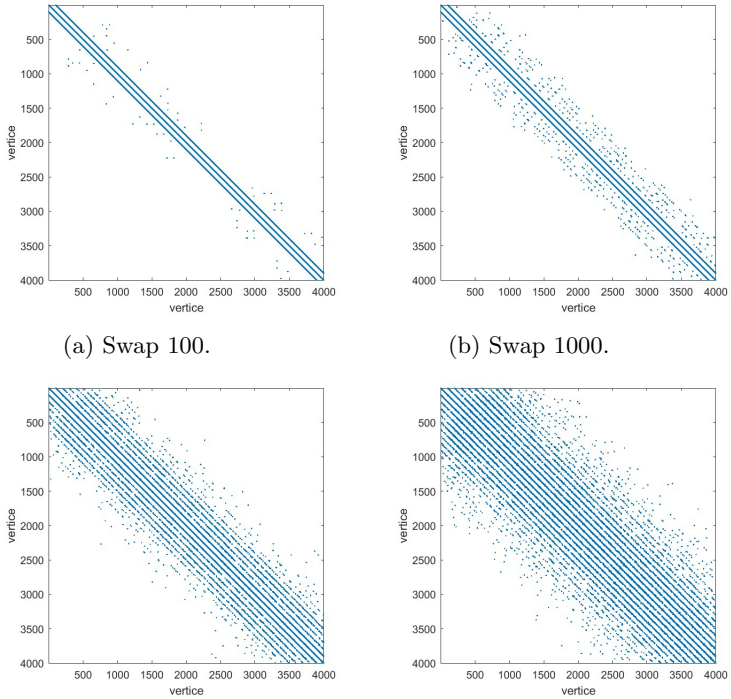

(a) Swap 100.

(b) Swap 1000.

(c) Swap 9000.

(d) Swap 35000.

Figure 19: Close up of the change in the left upper corner of the discrete Laplace matrix after 100, 1000, 9000 and 35000 swaps. The actual discrete Laplacian is a 15400×15400 matrix *Matlab*

The eigenvalues μ of matrix L only change very slowly and can therefore be 'followed' through the sequence of swaps by comparing the eigenvectors corresponding with the destabilising eigenvalues λ of the full system. In order to do so, we will need to find a relation between the eigenvalues μ of the discrete Laplacian and the eigenvalues λ of the full system. In the next section this relation is derived.

4.3.3 The discrete dispersion relation

We can derive the relation between the eigenvalues μ of the discrete Laplacian and the eigenvalues λ of the full system in the same way the dispersion relation between the wavenumber k and λ was found in Section 2.2.2.
Rewriting (93) the discrete system can be described in compact matrix form as

$$\lambda \overline{\chi w} = J_d \overline{\chi w} + D \overline{\chi w}, \tag{101}$$

where J_d is the discrete Jacobian (87) and D (88) contains the discrete Laplacian for both vectors u and v.
The eigenvalues λ of the full system can be computed by solving the characteristic equation. For every combination λ, μ, where μ is an eigenvalue of the discrete Laplacian L we have in terms of f_u, f_v, g_u and g_v

$$\det \begin{pmatrix} \mu + f_u - \lambda & f_v \\ g_u & \varepsilon^2 \mu + g_v - \lambda \end{pmatrix} = 0. \tag{102}$$

Therefore, the eigenvalues λ are solutions to the quadratic equation

$$\lambda^2 - (\mu(1+\varepsilon^2) + (f_u + g_v))\lambda + h(k^2) = 0 \tag{103}$$

$$\text{with} \quad h(k^2) = \varepsilon^2 \mu^2 + (\varepsilon^2 f_u + g_v)\mu + f_u g_v - f_v g_u, \tag{104}$$

and we find

$$\lambda_{-,+}(\mu) = \frac{(\mu(1+\varepsilon^2) + (f_u + g_v)) \pm \sqrt{(\mu(1+\varepsilon^2) + (f_u + g_v))^2 - 4h(k^2)}}{2}. \tag{105}$$

In this case, the eigenvalues λ of the full system depend on the eigenvalues μ of the discrete Laplacian. We can call this the *discrete dispersion relation*. The eigenvalues μ and $\lambda(\mu)$ are discrete and lie on the curves plotted in Figure 20a. The dotted lines in Figure 20b represent the boundaries of the interval $[\mu_-, \mu_+]$ in which the function $\mathrm{Re}(\lambda_+(\mu))$ is positive. Due to perturbations of the associated eigenvectors this leads to destabilisation of the uniform steady state. The eigenvectors corresponding to the positive eigenvalues λ_+ can be converted to the network and plotted.
All eigenvalues μ are negative, with largest value $\mu_0 = 0$. Because all row sums of the discrete Laplacian are zero, the matrix must have an eigenvalue that is zero. On the left hand side the graph is truncated but in reality it continues.

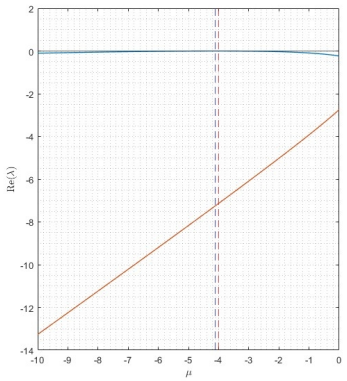

(a) Relation between the real part of eigenvalues $Re(\lambda_-)$ and $Re(\lambda_+)$ and μ.

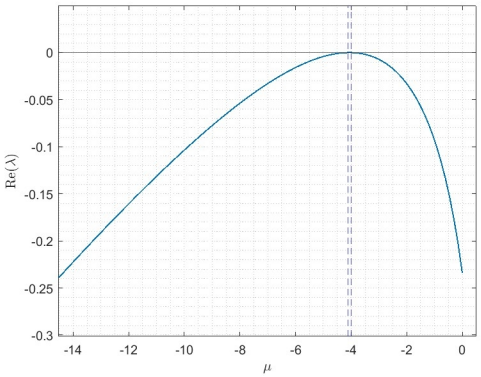

(b) Dispersion relation of $Re(\lambda_+(\mu))$.

Figure 20: Relation between the real part of eigenvalues λ and μ. The dashed lines are the upper and lower bound of the interval $[\mu_-, \mu_+]$ for which $\mathrm{Re}(\lambda)$ is positive.

Like in the continuous case, only one of the eigenvalues λ needs to be positive for the system to become unstable. We can compute the values of the interval $[\mu_-, \mu_+]$ in which this is the case like we did in the analytic case (75) by solving $h(\mu)$ (104) for μ.

$$\begin{aligned} \mu_- &= \frac{1}{2\varepsilon^2}[-(\varepsilon^2 f_u + g_v) - \sqrt{(\varepsilon^2 f_u + g_v)^2 - 4\varepsilon^2(f_u g_v - f_v g_u)}] < \mu \\ &< \frac{1}{2\varepsilon^2}[-(\varepsilon^2 f_u + g_v) + \sqrt{(\varepsilon^2 f_u + g_v)^2 - 4\varepsilon^2(f_u g_v - f_v g_u)}] = \mu_+ \end{aligned} \tag{106}$$

Because the discrete Laplace matrix is finite, its number of eigenvalues is finite. The eigenvalues μ of L are all negative with largest eigenvalue zero. As the discrete Laplacian changes by the swapping of edges, so do its eigenvalues μ, but only with very small steps. In Figure 21 every row displays portion of the eigenvalues of the network. All rows are 100 swaps apart, starting with the eigenvalues belonging the discrete Laplacian of the initial lattice on the bottom row, up to to the Laplacian of the network at swap 1100 at the top row. In Figure 21a, one of the smallest eigenvalues, depicted with a red star, is followed through the swap steps. The value of this specific eigenvalue μ_* increases as the network becomes more random. On the other side of the spectrum, in Figure 21b, another eigenvalue that belongs to the largest eigenvalues, is followed as its value decreases. If the smallest eigenvalues keep increasing in value, there must be one ore more regions in the spectrum where the density increases.

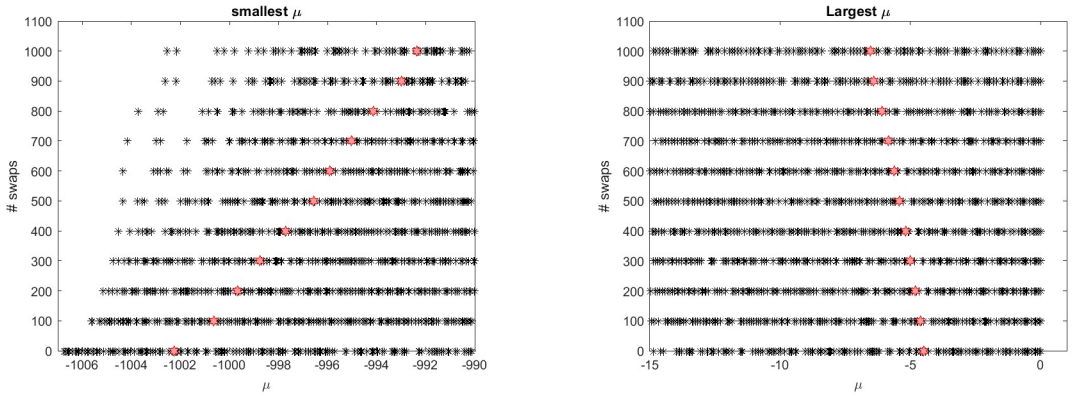

(a) Change of the smallest eigenvalues μ.

(b) Change of the largest eigenvalues μ.

Figure 21: The change of the smallest and largest eigenvalues μ of the discrete Laplacian as the number of swaps increases, plotted per 100 swaps. On each side of the spectrum, a single eigenvalue is indicated with a red star. Both eigenvalues are followed as one increases (a) in value and the other decreases in value (b).

For the remaining part of this section we will label the eigenvalues μ. We sort the eigenvalues according to their value from large to small and label them μ_0, μ_1, up to μ_{15400}. According to the discrete dispersion relation, there are two eigenvalues, λ_+ and λ_-, for every eigenvalue μ in Figure 21. The positive $\lambda_+(\mu)$ must lie on the curve of Figure 20. This is indeed the case. In Figure 22 the largest μ are depicted with black asterisks, with a largest eigenvalue that has value zero. One of the eigenvalues, μ^*, is marked with a red asterisk. The eigenvalues of the discrete Laplacian change with every performed swap, but the changes are small. The largest eigenvalues μ can be linked to themselves by comparing their eigenvectors in each swap. Matrix L changes during the experiment and its eigenvalues gradually change over time, except the largest μ_0, which will always be zero. The value of eigenvalue μ^* decreases as L changes. As long as the eigenvalue μ^* is to the right of the interval $[\mu_-, \mu_+]$, the value of $\mathrm{Re}(\lambda(\mu^*))$ is negative but increases as μ^* decreases. In this stage the uniform steady state is stable against non-homogeneous perturbations. When μ^* passes through the interval, $\mathrm{Re}(\lambda(\mu^*))$ becomes positive and the steady state becomes unstable against these perturbations. Then the eigenvalue decreases again and leaves the interval the steady state becomes stable against spatial perturbations again.

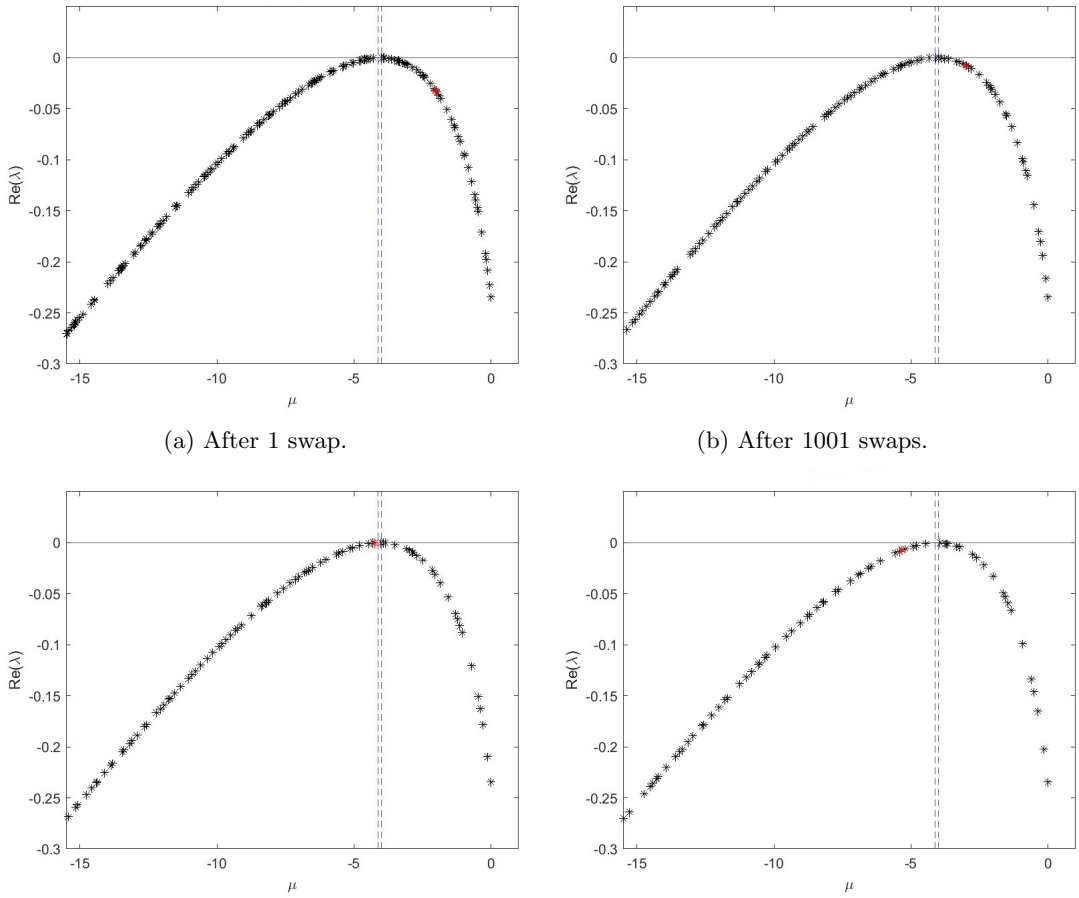

(a) After 1 swap.

(b) After 1001 swaps.

(c) After 2001 swaps.

(d) After 3001 swaps.

Figure 22: Real part of eigenvalues λ as a function of the distinct eigenvalues μ of the discrete Laplacian. One eigenvalue μ^* (red) is followed through the swap steps as it passes through the interval for which $\text{Re}(\lambda)$ is positive. The dashed lines are the upper and lower bound of this interval *Matlab*.

4.3.4 Correlation between distance and change in eigenvalues

From the difference in distance between the eigenvalues in each step in Figure 21 it can be deduced that the step size of the changes of the μ is not constant. There are two hypothesis for the size of the change in μ_i.

1 The location of the swap in the domain determines the size of the change of μ_i. This is the distance from the centre of the domain, the global distance *gd*.

2 The distance between the two edges that are being swapped, which we call the local distance *ld*, determines the size of the change of μ_i.

We recorded the exact locations of all four vertices that are involved in a swap in the network. With these locations, the Euclidean distance between the centre of the network and the centre of all nodes involved can be computed for every swap that is performed. In hypothesis 1, the x-coordinate of the location of the swap is defined as one fourth of the sum of the coordinates of all four nodes in the x-direction and the y-coordinate as one fourth of the sum of the coordinates of all four nodes in the y-direction. The global distance is then the Euclidean distance between the centre of the swap and the centre of the network. That means that every swap with global distance *gd* is equally far from the origin, but not necessarily equally far from a boundary of the network, because the Euclidean

distance is circular, while the domain is rectangular. The results over the first 11.000 time steps are in Figure 23a. The black line denotes a least square linear fit of the data. We found no relation between the global distance and the change of the eigenvalue λ. The global distance is a very rough estimate that does not tell us much about the distance to the boundary. Comparing the global location to the location in the discrete Laplacian, it is understandable why there is no correlation; the new location in the Laplacian relative to the distance to the diagonal of the matrix does not depend on the location in the network. Therefore there is no greater impact of a swap being close to the centre of the network and one at the boundary of the network.

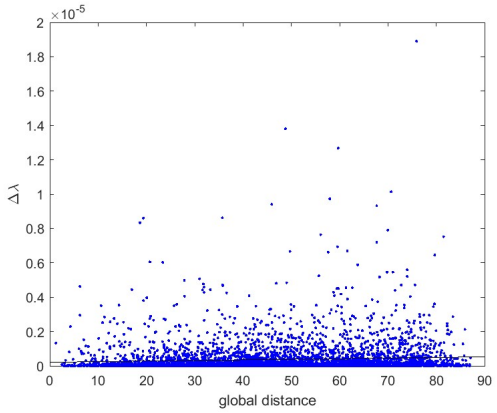

(a) Relation global distance of the edges of the swap to the centre of the network with the size of the difference in eigenvalue λ_+.

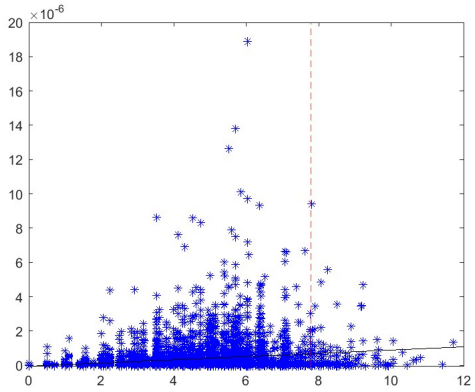

(b) Relation local distance between the edges of the swap with the size of the difference in eigenvalue λ_+. The dashed red line indicates the bound on the distance between the two swapped edges as in rule (3) from Section 3.2.1.

Figure 23: Global and local correlation of the edge distances with the change in eigenvalue size of λ_+ for the first 11000 swaps. *Matlab*

The local distance is found by computing the Euclidean distance between the middle of the two edges that are swapped. In section 3.2.1 the maximum distance between two edges that were allowed to be swapped was derived to be $7.78h$. But if edges that were created in a previous swap are involved, then this distance can be larger. That this happens can be seen in Figure 23b where this critical value is shown as a vertical red dashed line. Also data points on the left side of this line could be swaps involving previously formed new edges. Applying linear least squares shows that there is a correlation between the local distance of the swap and the change of the eigenvalue λ_+.

4.3.5 Reaction diffusion on the changed network

In this section we will look at the effect of the edge swaps on the eigenvectors of the system, specifically on the patterns that are formed on the two dimensional domain. We will see that the order in which the pattern appears can often be predicted and linked to the analytical case where, instead of swapping edges, in each step the size of the domain is decreased by a small factor the while ratio $lx : ly$ stays constant.
First we analyse the changed system. The eigenvalues of the discrete Laplacian pass through the interval $[\mu_-, \mu_+]$.
To visualise this, in each time step the location of the swap and the positive eigenvalues λ of the reaction diffusion system on the resulting network are saved. The corresponding eigenvector is plotted and the eigenvalue μ of the discrete Laplace operator that causes the pattern, is followed through time. In Figure 24 the real part of all found positive eigenvalues λ for the first 700 swap steps are plotted against the swap number. The colours were added after hand-sorting the patterns. This involves

looking at all the patterns in each swap and determining which ones belong together over the course of the process, and therefore belong to the same eigenvalue. Similar patterns are given the same colour. As a result the path of the discrete dispersion relation that the eigenvalues follow is clearly visible, even if the path is occasionally irregular. Some swaps cause big jumps of the destabilising eigenvalues. For example, the positive eigenvalue that appears in swap 343 in Figure 24b has a large initial value. Even larger jumps can be made if the swap alters the network severely enough.
This process seems straightforward, but eigenvectors of the discrete Laplacian belonging to $\lambda_+(\mu)$ now live on a three dimensional network instead of a two dimensional lattice, which makes the pattern hard to discern. As an alternative the eigenvector can be converted to the structure of the initial lattice. Because the swaps are local, all newly formed edges connect vertices that are relatively close and despite some of the neighbouring vertices no longer being connected the patterns are clearly visible.

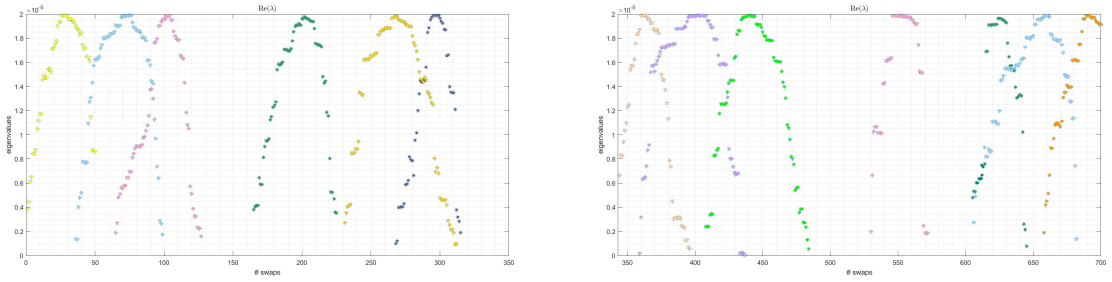

(a) Eigenvalues followed through swaps 1 to 343. (b) Eigenvalues followed through swaps 344 to 700.

Figure 24: First thirteen patterns for which the real part of the eigenvalue, $\mathrm{Re}(\lambda)$, is larger that zero, followed through the first 700 swaps.

The network can be plotted with values of v depicted in a color scale. In the first and third columns in Figure 25, six increasingly less regular networks are plotted, each at a different stage of the process.

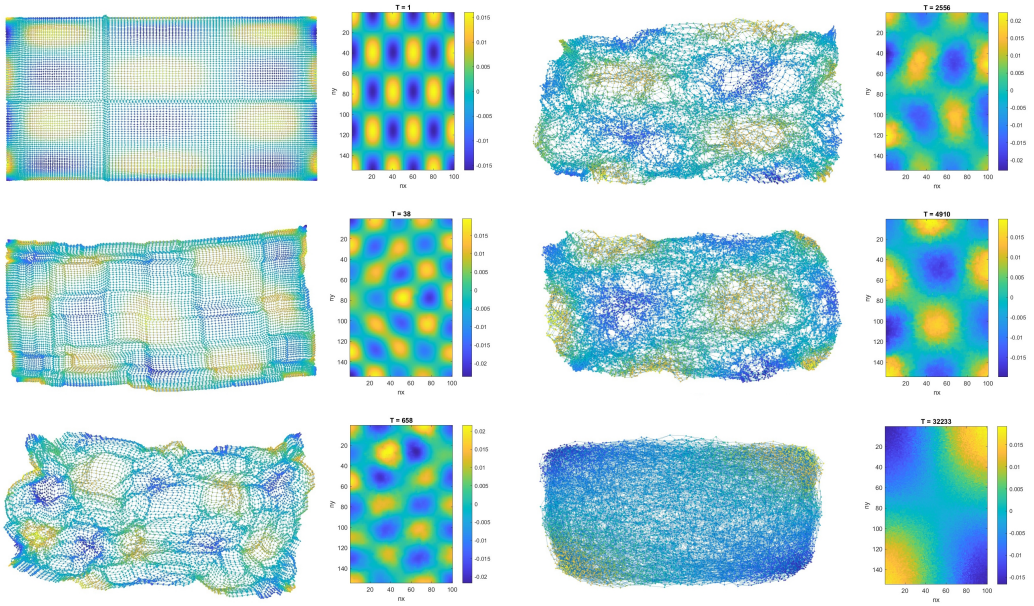

Figure 25: Discrete eigenvectors of six destabilising eigenvalues on the network as well as reconstructed to the original lattice. The plots were made at swap 1, 35 and 658 (left column, top to bottom) and swap 2500, 4969 and 31665 (right column, top to bottom).

As mentioned before, the patterns are not very easy to interpret on the three dimensional network. On top of that the build in Matlab program that plots the networks in 3D has a tendency to increase node density at the boundaries of the lattice. This means that the pattern is compressed at the boundaries. Therefore the projection of the pattern onto the initial lattice is plotted to the right of each network in the second and fourth column of Figure 25. The Matlab program also tends to rotate and flip the plot of the network which complicates the interpretation of the three dimensional image even further. We did not compensate for this and left the networks as plotted by Matlab.

We have used the same projection techniques to visualise the eigenvectors belonging to the thirteen eigenvalues $\lambda(\mu)$ of Figure 24. They are plotted in Figure 26 in the order in which they appear during the procedure. The first pattern to appear is the single initial possible pattern that was found analytically on the continuous domain and numerically on the initial lattice (Figure 15). The combinations (m, n) can be deduced from counting the number of times peaks (blue) and valleys (yellow) alternate horizontally and vertically. Each alternation represents a wavelengths ω. For patterns found later in the procedure this becomes increasingly difficult, or possible even. The combinations for the first five patterns in the top row, from left to right, in Figure fig:First13EVs are; (5,4), (4,6), (1,8), (3,7) and (5,3). After the fifth pattern, the wavelengths countable in at most one direction. The last two patterns in the bottom row have combinations (2,7) and (3,6).

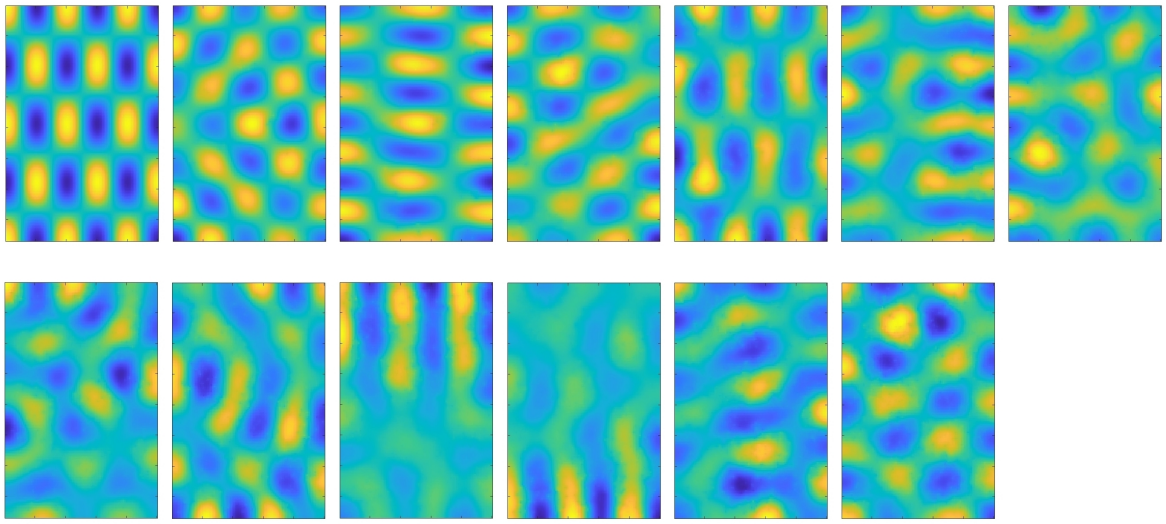

Figure 26: The eigenvectors corresponding to the thirteen destabilising eigenvalues found in Figures 24a and 24b, projected onto the initial lattice.

It is not the case that patterns become less recognisable when the networks becomes less regular. Even after 30,000 swaps, patterns made from the unstable eigenvectors are still very identifiable and their combinations (m, n) can be derived. The last pattern in Figure 26 from swap 31665 clearly has combination (1,1).
The discrete dispersion relation and Figure 22 suggest that the eigenvectors appearing on the network when they become unstable were already present in the initial lattice. To investigate this, we will compare the eigenvectors belonging to eigenvalues μ of the discrete Laplacian of the initial lattice with the unstable eigenvectors on the network. We plot all eigenvectors of the initial discrete Laplacian corresponding to eigenvalues μ larger than the initial eigenvalue that caused the first unstable eigenvalue in the initial lattice. These eigenvalues are depicted with red asterisks in Figure 27 and are equal to or larger than the initial eigenvalue μ in the interval $[\mu_-, \mu_+]$ of the initial lattice.

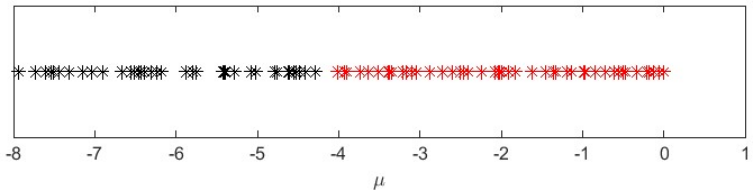

Figure 27: The largest eigenvalues μ of discrete Laplacian L of the initial regular lattice. The red asterisks are the eigenvalues μ larger than the value of the eigenvalue of the initial pattern $(5, 4)$.

As the network becomes further distorted most of the eigenvalues will pass through the interval $[\mu_-, \mu_+]$. The second and third largest eigenvalues μ_1 and μ_2 will not become large enough because the diameter of the network does not become small enough within the 35000 swaps of the experiment. It might pass through the interval if the number of swaps becomes large enough. The zero eigenvalue μ_0 will stay zero and therefore never become large enough to pass through the interval. The eigenvector belonging to the zero eigenvalue μ_0 is constant on the domain.

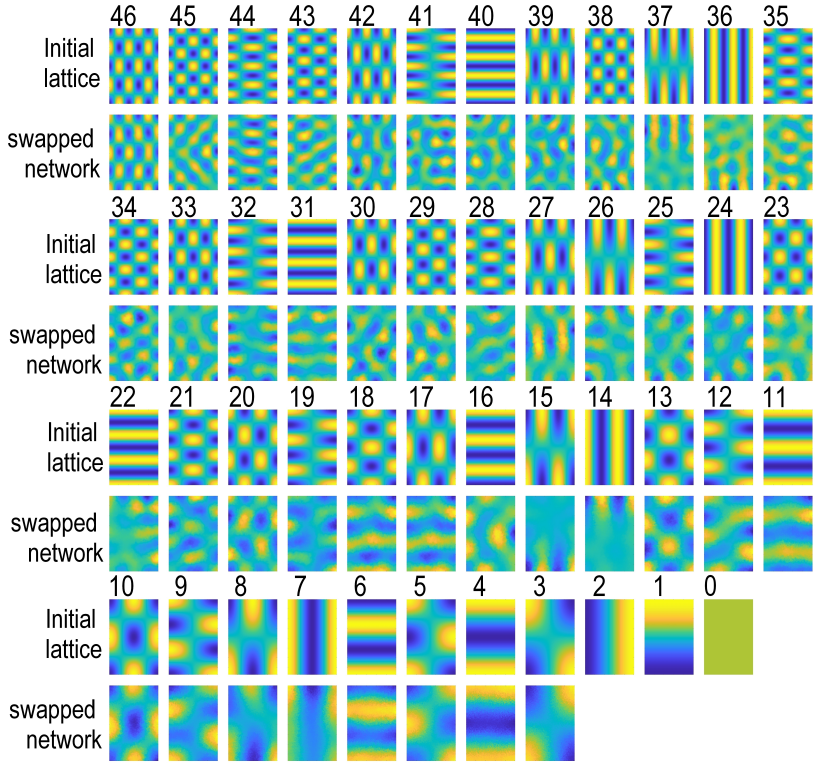

Figure 28: All stable eigenvectors of the discrete Laplacian of the initial lattice for the eigenvalues μ depicted with a red asterisk in Figure 27 compared to the unstable eigenvectors of the swapping process in order of appearance.

There are 47 eigenvalues μ in and to the right of the interval $[\mu_-, \mu_+]$. The eigenvectors of full system that correspond to the eigenvalues of the discrete Laplacian of the initial lattice, are numbered in order of the increasing value of μ, from 0 up to 47, just like the μ_i we defined before. The representation of the eigenvectors on the initial lattice are plotted in Figure 28. All of the eigenvectors are stable, except for initial destabilising eigenvector 46. Below each plot of a stable eigenvectors is a plot of a destabilised eigenvector of a network during the swap process. These are snapshots of the eigenvectors at their peak in the discrete dispersion relation, when the maximum value of their destabilising eigenvalue λ

is approximately 2×10^{-5}. The plots are arranged in order of appearance. If we ignore the phase of the patterns, some of them are clearly recognizable, especially at the end of the process when m and n become small.
In most cases, as the eigenvalues μ and λ change, the patterns produced by unstable eigenvectors do not change significantly. But it does happen that over the course of the existence of a pattern, the eigenvector changes in a way that the pattern can no longer identified. An example are patterns 18, 17 and 16 in Figure 29. The first pattern to appear is pattern 18 in swap 3274. At swap step 3275 the destabilising eigenvalue merges with a second eigenvalue, $\lambda(\mu_1 7)$, and both eigenvalues become complex. The real parts of their eigenvectors are identical and only one pattern can be discerned in the plots. During this phase the pattern changes and its eigenvalue $\lambda(mu)$ reaches it maximum value at swap 3333. The eigenvalues separate at swap 3347 with now two distinguishable patterns. What can also happen is that the patterns are no longer in the same order as the eigenvectors of the initial lattice. For example, pattern 17 and 16 seem to have switched order in Figure 28.

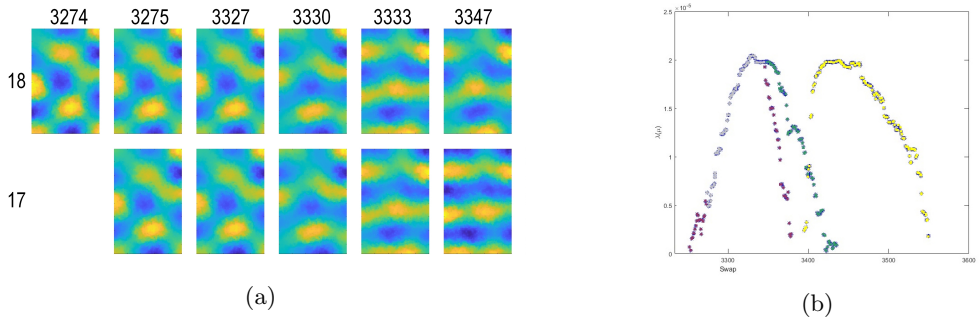

(a) (b)

Figure 29: Plot of the unstable eigenvalues λ as a function of μ showing patterns 18, 17 and 16. The unstable eigenvector of pattern 18 (purple) merges with a second unstable eigenvector at swap 3275 and the real part of both patterns continues as a single unstable pattern (grey). At swap 3347 the patterns separate.

Figure 25 shows some of the most identifiable patterns that emerge during the swapping procedure. On the original continuous domain, the wavenumbers these combinations of m and n produce would not be inside the interval (k_1^2, k_2^2). The values of k are too small and would only be destabilising on a domain that is smaller in size than our initial domain size. This raises the question whether we can compare the sequence of destabilising eigenvectors of the changing network with the unstable eigenfunctions of a continuous domain that that is smaller in size than the initial one. The answer will be given in the following section.

4.3.6 Relation swaps - lattice size

If the the unstable eigenfunctions the system on smaller domains have the same ordering as the numerically derived eigenvectors of the changing network, then perhaps a relation between the properties of the network and the size of the continuous domain can be found that connects both the analytically and numerically derived pattern sequence. First we will derive all 46 non uniform patterns from Figure 28 analytically by reducing the domain size was incrementally. In each step s, the initial horizontal and vertical sizes lx and ly of the domain were multiplied by $s/100000$ up to step $s = 100000$. All possible wavenumbers were collected in each step s. For larger domain size, multiple wavenumbers can appear at the same time and they persist for a large number of steps. For smaller domains, the overlap of the existing wavenumbers is much smaller and they persist for a shorter number of steps. All found patterns are plotted in Figure /reffig:AnalyticPatterns.

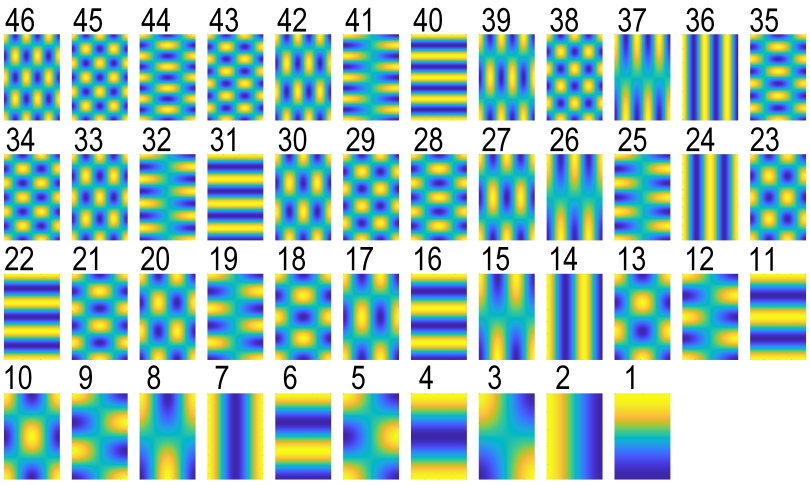

Figure 30: From left to right and top to bottom the analytical solutions for a decreasing domain size, from large domain to small.

The patterns for increasing swap steps of the discrete case in Figure 28 can be compared to the patterns for decreasing domain size in Figure 30.
The fact that the order of the patterns in the analytical case and the network case is almost identical suggests that there is a connection between a property of the changing network and some parameter of the analytical solution that has a connection with the decreasing domain sizes. There are two properties of interest in the discrete case, namely diameter and radius that both represent distance. In the case of the diameter it the length of the shortest path between the most distanced vertices. The only parameters concerning the domain that are needed for the analytical case are width and length of the domain, which are related to each other by their ratio.
For the derivation of the data points in Figure 31 the value of lx was measured at the centre of the interval in which they appear. These intervals are relatively small. The diameter was measured at the point where the unstable eigenvalue reaches its maximum value.

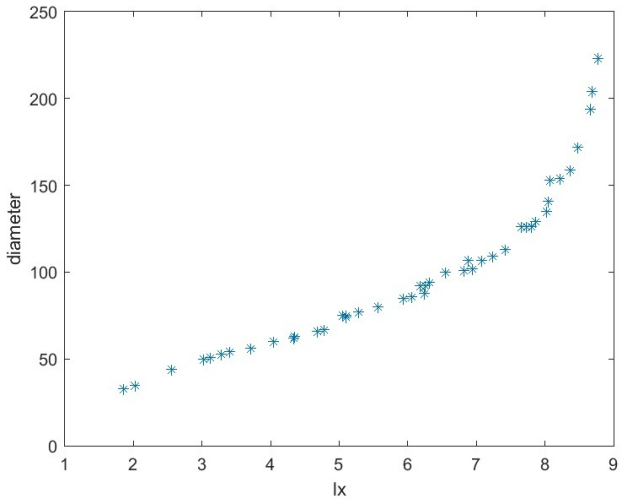

Figure 31: Correlation between the diameter of the network and the size of the domain.

The reaction-diffusion system posed on a network with a smaller diameter appears to exhibit the same behavior as when posed on a regular two-dimensional domain that is smaller in size.

5 Discussion

In this thesis we have studied the Klausmeier model on a rectangular domain, and on the sequence of networks that emerged after repeatedly braking two random edges and reconnecting the four nodes involved differently. We investigated the linear stability of the initial lattice and derived the discrete dispersion relation between the eigenvalues of the discrete Laplacian and the eigenvalues of the system. The destabilising eigenfunctions could be followed through the series of swaps by comparing their patterns projected on the initial lattice by eye. We have seen that increased randomisation to the network has a similar effect on the solutions of the discretised problem as decreasing the size of the domain has on the analytical solutions. In both cases the patterns that appeared were already present as eigenvectors of eigenvalues equal to or smaller than the one of the solution of the initial domain. These were eigenvalues of the discrete Laplacian in the case of the experiment, and wavenumbers of the Laplacian operator in the continuous case. To compare the size of the continuous domain to the randomness of the changing network, the minimum distance between the nodes of the network that are furthest apart was measured by computing the diameter of the graph. By plotting both lattice size and diameter of the same pattern at their first appearance, the relation between the analytical shrinking domain and the experiment was found. One could say that these new edges, or pathways, that replace the distance over multiple edges by just a single one, make the domain 'smaller', kind of in the way that increased mobility and digital connections have made the human world smaller. Despite the fact that we have the same number of nodes and the same number of edges, the patterns on the new network after a large number of time steps are much coarser than the pattern of the initial lattice.

This research project is only concerned with one specific reaction diffusion model on a very specific sequence of networks. Other models might yield different results, specifically if the shape of the discrete dispersion relation would be different. It would also be interesting to investigate the effects of the Klausmeier model on random graphs especially because they have no boundary conditions. When networks no longer have a spatial domain, the concept of a pattern is not that obvious (McCullen and Wagenknecht 2016). and differs from what we have seen on a two and three dimensional networks in this thesis.

All edges are equal, also the new ones, except for the ones with boundary conditions. The edges are without weights and all have length dx. A new edge bypasses other nodes and leads to faster diffusion for the species on the network. Like creating a short piece of highway between two nodes, but without entrances and exits to nodes at either side of the new highway. The more highway pieces, the faster a species, water of vegetation, can diffuse from one side of the lattice to the other. The decrease of the diameter in the experiment proofs exactly that. In other words, the ratio between the impact of diffusion and that of the reaction equations changes to the benefit of the diffusion.

The deletion of edges could represent animal- or man-made obstacles and reconnecting the vertices the transportation routes that can increase or decrease the distances that species, or in this case vegetation and water, spread across the domain in a single time step. Examples of such obstacles and transportation routes are dams and canals respectively. But roads and railways can also increase the dispersal of plant seeds, for example by mud with seeds in it, that sticks to the wheels and the vehicles that use these routes (Hodkinson and Thompson 1997). They can also provide a corridor in the form of a road verge (Tikka, Högmander, and Koski 2001), which also facilitates the diffusion of species to distant places. These last two examples are interesting from an ecological point of view. In the experiment, however, considerably more new pathways are constructed than just a single stretch of highway which makes an increase of new edges in a natural landscape very hard to imagine.

The execution of the experiment itself can be improved. In section 3.2.1 the definition of a swap was given, with maximum swap distance between at least one of the nodes on each edge of $5dx$ in both the horizontal and vertical direction. From Figure 23b we can deduce that very often there are swaps with edges that were formed in a previous swap. A maximum distance of 5 in x and y direction between the centres of the edges that are being swapped would have truncated the plot in Figure 23b at the dashed red line. Most swaps have a minimal effect on the change of the observed destabilising eigenvalue $\lambda(\mu)$.

The dots beyond the red line give a distorted view of the relation of the distance between the edges of the swap with the change in size of the eigenvalue. We expect that with stronger bounds on the size of the swaps by this new definition, the decrease of the diameter would slow down and the relation would be more clear. For smaller swap distance the eigenvalues would pass through the domain $[\mu_1, \mu_2]$ at a slower rate. The swap distance could be a parameter depending on the real life process that it models.

Another improvement that could be made is the way the reconnection of the edges is defined, which is now very specific. Two edges are chosen from the upper triangular part of the discrete Laplacian and replaced by a new edge in the rows and columns of the old edges combined (see Figure 13). The same procedure is applied to the images of these points mirrored in the diagonal of the matrix. There is however another way to reconnect the nodes if one of the edges is first mirrored into the diagonal of the matrix, and then both edges are reconnected like before. The reason this comes to mind is the question whether the network can become disconnected. There is no reason why this could not happen, other than it being very improbable. But the way edges are reconnected might be of influence to the probability.

Lastly we will discuss the decrease of the diameter. The last pattern that was predicted, $(m, n) = (0, 1)$, has not been found in the experiment. For this pattern to appear, the diameter must decrease sufficiently. That raises the question whether there is a lower bound to the diameter of a graph with these properties, say number of nodes and maximum degree $d = 4$. Then the next eigenvalue μ of the discrete Laplace operator will not have a positive eigenvalue λ. Another way to check whether the value of the second largest μ becomes small enough to pass through the interval $[\mu_1, \mu_2]$ is to find the interval to which all eigenvalues μ must converge if the network is completely randomised. The distribution of the spectrum of the graph Laplacian of a large random graph of degree four is known (McKay 1981). The network from this thesis will, when the number of swaps is sufficiently large, say N, eventually be a random graph of degree four. When the size of the network is large enough, the distribution might tell us where the supply of destabilising eigenvalues stops. If the interval and the distribution overlap, an eigenvalue becomes 'stuck' as a permanently destabilising factor.

References

Turing, A. (1952). "The chemical basis of morphogenesis". In: *Bulletin of Mathematical Biology* 52, pp. 153–197. URL: https://api.semanticscholar.org/CorpusID:937133.

McKay, Brendan D. (1981). "The expected eigenvalue distribution of a large regular graph". In: *Linear Algebra and its Applications* 40, pp. 203–216. ISSN: 0024-3795. DOI: https://doi.org/10.1016/0024-3795(81)90150-6. URL: https://www.sciencedirect.com/science/article/pii/0024379581901506.

Carlberg, R. and Wendy Freedman (Nov. 1985). "Dissipative models of spiral galaxies". In: *Astrophysical Journal - ASTROPHYS J* 298, pp. 486–492. DOI: 10.1086/163634.

Hodkinson, Dunmail J. and Ken Thompson (1997). "Plant Dispersal: The Role of Man". In: *Journal of Applied Ecology* 34.6, pp. 1484–1496. ISSN: 00218901, 13652664. URL: http://www.jstor.org/stable/2405264 (visited on 02/02/2024).

Klausmeier, Christopher A. (1999). "Regular and Irregular Patterns in Semiarid Vegetation". In: *Science* 284.5421, pp. 1826–1828. DOI: 10.1126/science.284.5421.1826. eprint: https://www.science.org/doi/pdf/10.1126/science.284.5421.1826. URL: https://www.science.org/doi/abs/10.1126/science.284.5421.1826.

Tikka, Päivi, Harri Högmander, and Piia Koski (Jan. 2001). "Road and railway verges serve as dispersal corridors for grassland plants". In: *Tikka, P.M., Högmander, H. and Koski, P.S. 2001. Road and railway verges serve as dispersal corridors for grassland plants. Landscape Ecology 16: 659–666, 2001.* 16. DOI: 10.1023/A:1013120529382.

Rietkerk, M et al. (Oct. 2002). "Self-organization of vegetation in arid ecosystems". English. In: *American Naturalist* 160.4, pp. 524–530. ISSN: 0003-0147. DOI: 10.1086/342078.

Libbrecht, Kenneth G. (2003). "Explaining the formation of thin ice crystal plates with structure-dependent attachment kinetics". In: *Journal of Crystal Growth* 258.1, pp. 168–175. ISSN: 0022-0248. DOI: https://doi.org/10.1016/S0022-0248(03)01496-9. URL: https://www.sciencedirect.com/science/article/pii/S0022024803014969.

Murray, J. D. (2003). *Mathematical Biology II: Spatial Models and Biomedical Applications*. Vol. 18. Interdisciplinary Applied Mathematics. Springer New York. DOI: 10.1007/b98869.

Rietkerk, Max, Stefan C. Dekker, et al. (2004). "Self-Organized Patchiness and Catastrophic Shifts in Ecosystems". In: *Science* 305.5692, pp. 1926–1929. DOI: 10.1126/science.1101867. eprint: https://www.science.org/doi/pdf/10.1126/science.1101867. URL: https://www.science.org/doi/abs/10.1126/science.1101867.

Herrmann, Hans-J. (2006). "Pattern Formation of Dunes". In: *Nonlinear Dynamics* 44.1, pp. 315–317. DOI: https://doi.org/10.1007/s11071-006-2016-3.

Gilad, E. et al. (2007). "A mathematical model of plants as ecosystem engineers". In: *Journal of Theoretical Biology* 244.4, pp. 680–691. ISSN: 0022-5193. DOI: https://doi.org/10.1016/j.jtbi.2006.08.006. URL: https://www.sciencedirect.com/science/article/pii/S0022519306003493.

Myint-U, Tyn and Lokenath Debnath (2007). "Eigenvalue Problems and Special Functions". In: *Linear Partial Differential Equations for Scientists and Engineers*. Boston, MA: Birkhäuser Boston, pp. 273–327. ISBN: 978-0-8176-4560-1. DOI: 10.1007/978-0-8176-4560-1_8. URL: https://doi.org/10.1007/978-0-8176-4560-1_8.

Sherratt, Jonathan A. and Gabriel J. Lord (2007). "Nonlinear dynamics and pattern bifurcations in a model for vegetation stripes in semi-arid environments". In: *Theoretical Population Biology* 71.1, pp. 1–11. ISSN: 0040-5809. DOI: https://doi.org/10.1016/j.tpb.2006.07.009. URL: https://www.sciencedirect.com/science/article/pii/S0040580906001134.

Stelt, Sjors van der et al. (Feb. 2013). "Rise and Fall of Periodic Patterns for a Generalised Klausmeier-Gray-Scott Model". In: *Journal of NonLinear Science* 23, pp. 39–95. DOI: 10.1007/s00332-012-9139-0.

Siteur, Koen et al. (Dec. 2014). "Beyond Turing: The response of patterned ecosystems to environmental change". In: *Ecological Complexity* 20, pp. 81–96. DOI: 10.1016/j.ecocom.2014.09.002.

Siero, E. et al. (Mar. 2015). "Striped pattern selection by advective reaction-diffusion systems: Resilience of banded vegetation on slopes". In: *Chaos: An Interdisciplinary Journal of Nonlinear Sci-*

ence 25.3, p. 036411. ISSN: 1054-1500. DOI: 10.1063/1.4914450. URL: https://doi.org/10.1063/1.4914450.

Kim, Sangwoo et al. (2016). "Hexagonal Patterning of the Insect Compound Eye: Facet Area Variation, Defects, and Disorder". In: *Biophysical Journal* 111.12, pp. 2735–2746. ISSN: 0006-3495. DOI: https://doi.org/10.1016/j.bpj.2016.11.004. URL: https://www.sciencedirect.com/science/article/pii/S0006349516310311.

McCullen, Nick and Thomas Wagenknecht (Jan. 2016). "Pattern Formation on Networks: From Localised Activity to Turing Patterns". In: *Scientific Reports* 6. DOI: 10.1038/srep27397.

Doelman, Arjen (Apr. 2019). "Pattern formation in reaction-diffusion systems, an explicit approach". In: *Complexity Science: An Introduction*. Ed. by Mark Peletier, Rutger van Santen, and Erik Steur. ISBN: 978-981-323-959-3. DOI: 10.1142/10973.

Bastiaansen, Robbin, Martina Chirilus-Bruckner, and Arjen Doelman (2020). "Pulse Solutions for an Extended Klausmeier Model with Spatially Varying Coefficients". In: *SIAM Journal on Applied Dynamical Systems* 19.1, pp. 1–57. DOI: 10.1137/19M1255665. URL: https://doi.org/10.1137/19M1255665.

Bastiaansen, Robbin, Arjen Doelman, et al. (Jan. 2020). "The effect of climate change on the resilience of ecosystems with adaptive spatial pattern formation". In: *Ecology Letters* 23. DOI: 10.1111/ele.13449.

Knabner, P. and L. Angermann (2021). *Numerical Methods for Elliptic and Parabolic Partial Differential Equations: With contributions by Andreas Rupp*. Texts in Applied Mathematics. Springer International Publishing. ISBN: 9783030793845. URL: https://books.google.nl/books?id=XTV0zgEACAAJ.

Rietkerk, Max, Robbin Bastiaansen, et al. (2021). "Evasion of tipping in complex systems through spatial pattern formation". In: *Science* 374.6564, eabj0359. DOI: 10.1126/science.abj0359. eprint: https://www.science.org/doi/pdf/10.1126/science.abj0359. URL: https://www.science.org/doi/abs/10.1126/science.abj0359.

Herzog, Manuel et al. (2022). "Capturing complex star dune dynamics—repeated highly accurate surveys combining multitemporal 3D topographic measurements and local wind data". In: *Earth Surface Processes and Landforms* 47.11, pp. 2726–2739. DOI: https://doi-org.proxy.library.uu.nl/10.1002/esp.5420. eprint: https://onlinelibrary-wiley-com.proxy.library.uu.nl/doi/pdf/10.1002/esp.5420. URL: https://onlinelibrary-wiley-com.proxy.library.uu.nl/doi/abs/10.1002/esp.5420.